https://doi.org/10.5194/gmd-2022-236
Preprint. Discussion started: 2 January 2023

Geoscientific Model Development Discussions

Linking global terrestrial and ocean biogeochemistry with process-based, coupled freshwater algae-nutrient-solid dynamics in LM3-FANSY v1.0

Minjin Lee[1], Charles A. Stock[2], John P. Dunne[2], Elena Shevliakova[2]

[1]Program in Atmospheric and Oceanic Sciences, Princeton University; Princeton, NJ 08540, USA
[2]NOAA/Geophysical Fluid Dynamics Laboratory; Princeton, NJ 08540, USA

Correspondence to: Minjin Lee (minjinl@princeton.edu)

Abstract. Estimating global river solids, nitrogen (N), and phosphorus (P), in both quantity and composition, is necessary for understanding the development and persistence of many harmful algal blooms and hypoxic events. This requires a comprehensive freshwater model that can resolve intertwined algae, solid, and nutrient dynamics, yet previous global watershed models do not mechanistically resolve instream biogeochemical processes. Here we develop a global, spatially explicit, process-based, Freshwater Algae, Nutrient, and Solid cycling and Yields (FANSY) model and incorporate it within the Land Model LM3. The resulting model, LM3-FANSY, explicitly resolves interactions between algae, N, P, and solid dynamics in rivers and lakes at 1 degree spatial and 30 minute temporal resolution. Simulated solids, N, and P in multiple forms (particulate/dissolved, organic/inorganic) agree well with measurement-based yield (kg km^{-2} yr^{-1}), load (kt yr^{-1}), and concentration (mg l^{-1}) estimates across world major rivers. Furthermore, simulated global river loads of suspended solid, N, and P in different forms to the coastal ocean are consistent with published ranges. River N loads are estimated to be approximately equally distributed among forms with particulate organic, dissolved organic, and dissolved inorganic N accounting for 37%, 34%, and 30% respectively. For river P load estimates, particulate P, which includes both organic and sorbed inorganic forms, is the most abundant form (58%), followed by dissolved inorganic and organic P (32% and 10%). Analyses of model results and sensitivity to components, parameters, and inputs suggest that the fidelity of simulated river nutrient loads and N:P ratios with observation-based estimates could be improved markedly with better global estimates of nutrient inputs to rivers, including soil and litter runoff, wastewater, and weathering. Sensitivity analyses further demonstrate the role of algal dynamics in controlling the ratios of inorganic and organic nutrient forms. LM3-FANSY can serve as a baseline for linking global terrestrial and ocean biogeochemistry in next generation Earth System Models aimed at understanding the effects of terrestrial perturbations on coastal eutrophication under unprecedented socioeconomic and climate changes, where novel conditions challenge empirical approaches. Continued model enhancements will focus on the inclusion of terrestrial P dynamics, freshwater carbon and alkalinity dynamics, and anthropogenic hydraulic controls.

https://doi.org/10.5194/gmd-2022-236
Preprint. Discussion started: 2 January 2023


Geoscientific Model Development Discussions

1 Introduction

Dramatic increases in fossil fuel combustion, deforestation, agriculture, fertilizer use, and sewage outflows have increased loadings of terrestrial sediments and nutrients (e.g., nitrogen (N), phosphorus (P)) to rivers and coastal waters and changed N:P ratios (Cordell et al., 2009; Fowler et al., 2013; Lee et al., 2019; Sytvitski et al., 2005). These changes in sedimentary and nutrient loadings have altered turbidity and biogeochemistry in many freshwater and coastal ecosystems, which in turn have been linked to myriad consequences, including changes in ecosystem productivity and carbon (C) exports (Liu et al., 2021), increases in frequency, duration, and severity of harmful algal blooms (HABs) (Anderson et al., 2002; Heisler et al., 2008; Paerl et al., 2018) and hypoxic dead zones (Diaz and Rosenberg, 2008), and perturbations of aquatic plant, seagrass, and coral reef ecosystems, incurring substantial socioeconomic costs (Lacoul and Freedman, 2006; McLaughlin et al., 2003; Restrepo et al., 2006).

Resolving prominent drivers of the aforementioned aquatic ecosystem consequences requires a comprehensive freshwater biogeochemistry model. In general, strong positive relationships have been observed between P and phytoplankton production in freshwaters, while N increases have been linked with the development of large algal blooms and hypoxic events in estuarine and coastal waters (Howarth and Marino, 2006; Smith, 2003). In particular, inorganic nutrients, which are characterized by higher bioavailability than organic forms (Sipler and Bronk, 2004), have been recognized as critical drivers of algal blooms (including non-HABs) and hypoxic events (Kemp et al., 2005). Meanwhile, shifts in community composition towards more toxic or harmful algal species have often been attributed to changes in nutrient supply ratios, including N:P (Anderson et al., 2002; Heisler et al., 2008) and relative abundance of different N and P forms (e.g., nitrate (NO_3, Parsons et al., 2002), ammonium (NH_4, Trainer et al., 2007; Leong et al., 2004), urea (Glibert et al., 2001; Glibert and Terlizzi, 1999), dissolved inorganic N and P (DIN and DIP, Glibert et al., 2008)). Such shifts can be explained by differences in algal species-specific nutrient acquisition pathways that are controlled by nutritional status and preferences, uptake capability, and physiological status (Anderson et al., 2002). Furthermore, nutrient and algae dynamics are strongly linked with solid dynamics through phosphate (PO_4) sorption/desorption interactions with solid particles (McGechan and Lewis, 2002) and algae growth reduction due to light shading by suspended solids (SS) (Dio Toro, 1978). Estimating river solids, N, and P in both quantity and composition resulting from intertwined algae, nutrient, and solid dynamics is thus necessary for understanding the development and persistence of many HABs and hypoxic events.

Projecting global freshwater biogeochemistry changes requires process-based models that are robust under unprecedented conditions expected in the next century. Prior applications of process-based freshwater biogeochemistry models, such as RIVE (Billen et al., 1994) and QUAL2K (Pelletier et al., 2006), have generally been limited to small watersheds. Modeling river nutrient yields/loads on a global scale, in both magnitude and form, has been challenged by the difficulty of balancing desired details of instream biogeochemical processes along with limitations imposed by available knowledge, input and

https://doi.org/10.5194/gmd-2022-236
Preprint. Discussion started: 2 January 2023


Geoscientific Model Development Discussions

validation datasets. Global NEWS (Mayorga et al., 2010) and IMAGE-GNM (Beusen et al., 2016) are widely known global watershed models for simulating river nutrient yields/loads on a global scale. Global NEWS estimates have been shown to be consistent with measurement-based estimates across world major rivers, and provided important nutrient inputs for global ocean biogeochemistry model simulations. Global NEWS and IMAGE-GNM, however, do not resolve coupled algae, nutrient, and solid dynamics in freshwaters despite the intertwined relationships between the elemental cycles. Global NEWS 2, representing a hybrid of empirical, statistical, and mechanistic components, formulates and implements different elements and their chemical forms independently based on basin-averaged properties. IMAGE-GNM applied at a global scale does not differentiate dissolved, particulate, inorganic, and organic nutrient forms. Global applications of both models do not mechanistically resolve instream biogeochemical processes.

Prior global watershed models are also limited in their capacity to represent nutrient storage in terrestrial plants and soils. Global NEWS assumes that nutrients are in steady state and do not accumulate on land. IMAGE-GNM takes a mass balance approach to calculate soil nutrient budgets, which at times rests on simple scaling without potential dynamical feedbacks (e.g., an estimation of litter from floodplains to rivers as 50% of total net primary production (Beusen et al., 2015)). Simulations of soil organic nutrient delivery to rivers, however, depend to a great extent on the capability of models to simulate vegetation and soil organic nutrient storage in response to many terrestrial dynamics (e.g., vegetation growth, leaf fall, natural and fire-induced mortality, soil microbial processes) under long-term (multi decadal to centurial) historical climate and land use changes. Terrestrial storage changes have been shown to significantly alter multi-decadal river nutrient trends (Van Meter et al., 2018; Lee et al., 2019) and seasonal to multi-year river nutrient extremes (Kaushal et al., 2008; Lee et al., 2016; Lee et al., 2021).

Here we address limitations of previous models by developing a global, spatially explicit, process-based, Freshwater Algae, Nutrient, and Solid cycling and Yields (FANSY) model, and incorporate it within the National Oceanic and Atmospheric Administration (NOAA)/Geophysical Fluid Dynamics Laboratory (GFDL) Land Model LM3 which is capable of resolving coupled water, C, and N dynamics and storage changes in a vegetation-soil system (Lee et al., 2014; Lee et al., 2019). The resulting coupled terrestrial-freshwater biogeochemistry model LM3-FANSY constitutes a significant step toward a more process-based representation of the coupled, freshwater algae, nutrient, and solid dynamics linking global terrestrial and ocean biogeochemistry towards next generation Earth System Models. Here we provide a detailed model description, performance assessment against measurement-based global and regional estimates across world major rivers, and sensitivity evaluation to a range of components, parameters, and inputs.

https://doi.org/10.5194/gmd-2022-236
Preprint. Discussion started: 2 January 2023


Geoscientific Model Development Discussions

2 Model description

2.1 LM3-FANSY framework

LM3-FANSY is an expansion of NOAA/GFDL LM3-Terrestrial and Aquatic Nitrogen (TAN) (Lee et al., 2014; Lee et al., 2019) to include a terrestrial soil erosion process and comprehensive freshwater sediment and biogeochemical dynamics (Sect. 2.2). The terrestrial component LM3, which has been described in detail elsewhere (Gerber et al., 2010; Milly et al., 2014; Shevliakova et al., 2009), captures coupled water, C, and N dynamics within a vegetation-soil system. LM3 simulates transfers and transformations of three N species (i.e., organic, NH_4, and nitrate plus nitrite (NO_{23})) for vegetation and soil systems, considering the effects of anthropogenic N inputs, land use, atmospheric CO_2, and climate over timescales of hours to centuries. LM3 simulates the distribution of five vegetation functional types (C3 and C4 grasses, temperate deciduous, tropical, and cold evergreen trees) based on prevailing climate conditions and C-N storage in vegetation including leaves, fine roots, sapwood, heartwood, and labile storage. There are 4 soil organic pools (fast/slow litter and slow/passive soil) and 2 soil inorganic pools (NH_4 and NO_{23}). Scenarios of land use states and transitions are used to simulate four land use types (primary lands – lands effectively undisturbed by human activities, secondary lands – abandoned agricultural land or regrowing forest after logging, croplands, and pastures). LM3 captures key terrestrial dynamics that affect the state of vegetation and soil C-N storage, such as vegetation growth, leaf fall, natural and fire induced mortality, deforestation for agriculture, wood harvesting, reforestation after harvesting, and various soil microbial processes. LM3 extended to include a global river routing and lake model (Milly et al., 2014) is thus well suited to simulate the delivery of terrestrial N to rivers and coastal waters.

The terrestrial component LM3, including the newly added soil erosion process (Sect. 2.2.1), receives N inputs of fertilizer applications and atmospheric deposition, simulates biological N fixation, and estimates N outputs including net harvest (N in harvested wood, crops, and grasses after subtracting out internally recycled inputs, e.g., manure applied to croplands and sewage), emissions to the atmosphere, and eroded sediment and N runoff from terrestrial to river systems. In addition to terrestrial runoff of three N species (dissolved organic N (DON), NH_4, and NO_{23}) introduced in our previous study (Lee et al., 2014), here we have added particulate organic N (PON) runoff from the terrestrial fast and slow litter pools as described in the next section. Lee et al (2014, 2019) provides further details on the terrestrial model.

The freshwater component FANSY receives N, P, and solids in multiple forms either from LM3 (i.e., nutrient and sediment runoff from terrestrial soil and litter pools) or from prescribed inputs (e.g., sewage, aquaculture) and simulates biogeochemical transformations and transport of each form of the nutrients and solids within streams, rivers, and lakes (Sect. 2.2). N inputs to rivers from sewage, aquaculture, and atmospheric deposition, along with all P inputs, are specified in Sect. 3.1.

https://doi.org/10.5194/gmd-2022-236
Preprint. Discussion started: 2 January 2023


Geoscientific Model Development Discussions

2.2 Freshwater component FANSY

FANSY constituents of algae, nutrients, and solids in rivers and lakes are listed in Table 1 and described in Fig. 1. FANSY has 13 prognostic state variables and 6 diagnostic state variables. SS are delivered from the terrestrial soil detachment dynamics and generated from the death of algae described in Sect. 2.2.1. Particulate organic matter (POM, i.e., detritus or nonliving organic SS) and inorganic SS (ISS) are diagnosed from SS. SS dynamically interacts with bottom sediment (Sed) through deposition and suspension processes. Primary interactions between SS and other model components are through the shading effect of turbidity on algae growth (Sect. 2.2.2) and the sorption of PO_4 to inorganic suspended particles (i.e., ISS) as particulate inorganic P (PIP) (Sect. 2.2.4). Algae take up N and P, which is subsequently partitioned between organic and inorganic N and P pools via algae mortality (Sect. 2.2.2). Algae chlorophyll a (CHL), algae C (Ca), algae P (Pa), and algae dry matter (Da) are diagnosed from algal N (Na) and, in the case of CHL, nutrient and light conditions. The 5 prognostic N variables contain an oxidized and reduced dissolved inorganic forms (NO_{23} and NH_4), as well as dissolved and two particulate (suspended and sedimentary) organic forms (DON, PON, and sedimentary organic N (SedN), Sect. 2.2.3). The 5 prognostic P variables include the same organic forms as for N (dissolved organic P (DOP), particulate organic P (POP), and sedimentary organic P (SedP)), but includes dissolved and particulate inorganic forms (PO_4 and PIP, Sec. 2.2.4) rather than the oxidation state distinction as done for N. FANSY does not distinguish between PO_4, dissolved inorganic P (DIP), and soluble reactive phosphorus (SRP). The subsections that follow (Sect. 2.2.1-2.2.4) provide a detailed description of each of these variable processes.

Variable	Symbol
Prognostic variable	
Suspended solids	SS
Sediment solids	Sed
Algae nitrogen	Na
Ammonium nitrogen	NH_4
Nitrate plus nitrite nitrogen	NO_{23}
Phosphate (dissolved inorganic phosphorus or soluble reactive phosphorus)	PO_4 (DIP or SRP)
Particulate organic nitrogen	PON
Sediment nitrogen	SedN
Dissolved organic nitrogen	DON
Particulate organic phosphorus	POP
Sediment phosphorus	SedP
Dissolved organic phosphorus	DOP
Particulate inorganic phosphorus	PIP

https://doi.org/10.5194/gmd-2022-236
Preprint. Discussion started: 2 January 2023

Geoscientific Model Development Discussions

Diagnostic variable	
Particulate organic matter (detritus or nonliving organic suspended solids)	POM
Inorganic suspended solids	ISS
Algae phosphorus	Pa
Algae carbon	Ca
Algae dry matter	Da
Chlorophyll a	CHL

Table 1: Model prognostic and diagnostic variables.

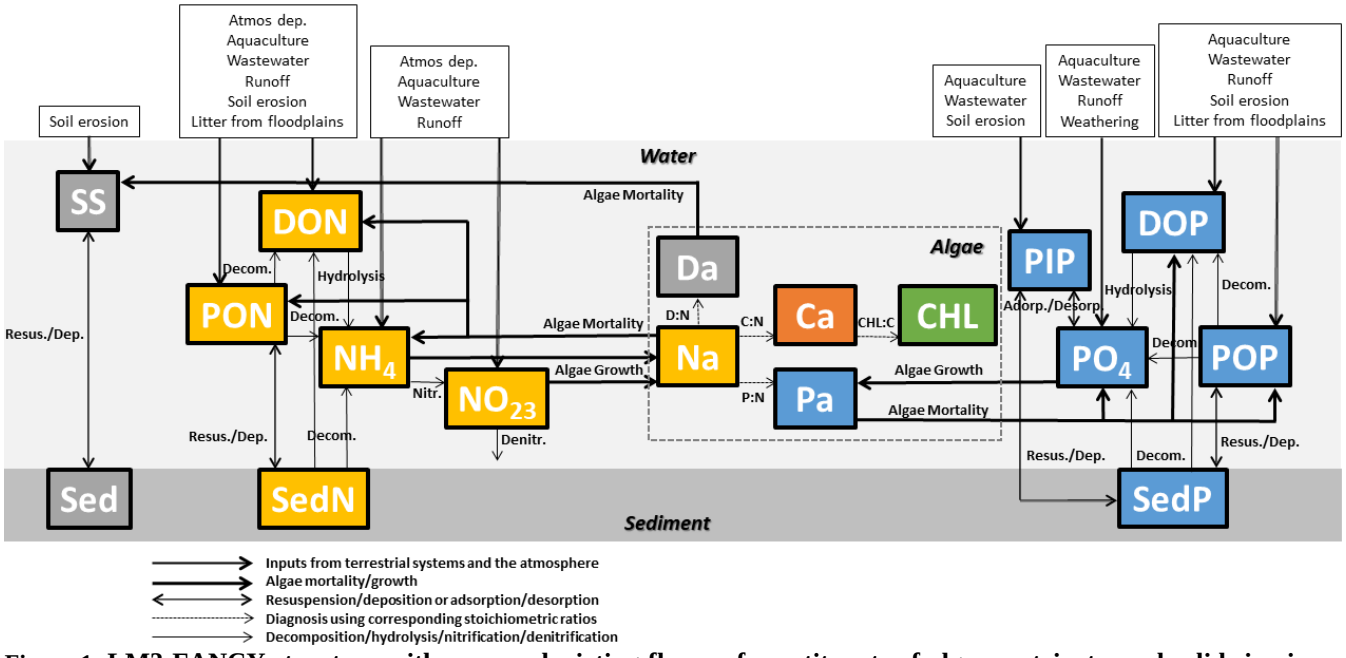

Figure 1: LM3-FANCY structure with arrows depicting fluxes of constituents of algae, nutrients, and solids in rivers and lakes. The constituents are listed in Table 1.

Added solids and nutrients to streams and rivers are subject to retention within rivers and lakes or transformed during transport to the coastal ocean. Freshwater physics, hydrology, and hydrography are described in detail elsewhere (Milly et al., 2014). Each model grid cell contains one river reach and/or one lake. Water containing solids and nutrients in each river reach or lake flows to another river reach in the downstream grid cell following a network that ultimately discharges to the ocean (Milly et al., 2014). In each river reach or lake, for each species, settling/resuspension dynamics and/or biogeochemical reactions (R_i) are calculated according to the process-based formulations described in the following

https://doi.org/10.5194/gmd-2022-236
Preprint. Discussion started: 2 January 2023

Geoscientific Model Development Discussions

subsections. A general mass balance for a species in a river reach or lake at each computation time step (30 minutes in this study) is written as:

$$\frac{dX_i}{dt} = F_i^{in} - F_i^{out} + I_i + R_i \,, \qquad \text{if i is a species from the river or lake water column} \qquad (1)$$

$$\frac{dX_i}{dt} = R_i \,, \qquad \text{if i is a river or lake benthic sediment species} \qquad (2)$$

where i is a species listed in Table 1, X_i is the amount of species i (kg), F_i^{in} and F_i^{out} are inflow and outflow of the species i (kg s^{-1}), I_i is inputs of the species i from terrestrial systems and the atmosphere (kg s^{-1}), and R_i is settling/resuspension dynamics and/or biogeochemical reactions of the species i (kg s^{-1}).

2.2.1 Solid dynamics

In LM3-FANSY, the detachment of soil from river basins is controlled by land surface slope, rainfall, and leaf area index (LAI), based on Pelletier (2012).

$$E = C_1 \cdot \frac{\rho_b}{\rho_w} \cdot S^{5/4} \cdot R \cdot e^{-L} \,, \qquad (3)$$

where E is terrestrial soil erosion rate (Dry matter (D)kg m^{-2} s^{-1}), C_1 is calibrated to measurement-based river SS estimates (unitless), ρ_b is soil bulk density (kgD m^{-3}), ρ_w is water density(kg m^{-3}), S is slope tanθ, with θ as hillslope angle (unitless), R is rainfall (kg m^{-2} s^{-1}), and L is LAI (unitless). Model parameters are described in Table 2. Soil detachment is known to be scale dependent, because it could be dominated by different spatial scale processes (e.g., interrill, rill, and gully erosion, landsliding, Poesen et al., 1996; Renschler and Harbor, 2002). We thus include a degree of freedom via the coefficient of C_1 that can be calibrated to account for spatial resolution of the input data (e.g., slope at the 1 degree scale). C_1 is a single global value and coarsely calibrated to match measurement-based estimates of river SS yields, loads, and concentrations across world major basins. Sensitivity of the model to C_1 is addressed later. It has been suggested to model soil detachment at event scales (daily or subdaily time steps) to account for episodic, substantial mass transport (Tan et al., 2017). We calculate soil detachment rate at the finest model time step (30 minutes).

Parameter	Description	Value	Unit	Reference/Rationale
T_{ref}	Reference temperature	20	°C	Many reactions are reported at 20°C.
θ	Temperature correction factor	1.066	unitless	Eppley (1972)
C_1	Free parameter of terrestrial soil detachment	0.015	unitless	Pelletier (2012); Calibrated to match measurement-based river SS estimates
κ	Karman constant	0.4	unitless	Pelletier (2012)
R	Submerged specific gravity	1.65	unitless	Ferguson & Church (2004)

https://doi.org/10.5194/gmd-2022-236
Preprint. Discussion started: 2 January 2023

Geoscientific Model Development Discussions

d	Grain diameter	0.01	m	
υ	Kinematic viscosity	$1\ 10^{-6}$ at 20 ℃	$m^2\ s^{-1}$	
C_2, C_3	Reported constants in the estimation of settling velocity	18, 1.0	unitless	
r_{DN}	Algae D-to-N ratio	13.9	$gD\ gN^{-1}$	Chapra (1997)
r_{DC}	Algae D-to-C ratio	2.5	$gD\ gC^{-1}$	
r_{CN}	Algae C-to-N ratio	5.56	$gC\ gN^{-1}$	
r_{PN}	Algae P-to-N ratio	0.14	$gP\ gN^{-1}$	
ζ	Cost of biosynthesis	0.05	unitless	Geider et al (1997)
α^{CHL}	Chlorophyll a-specific initial slope of the photosynthesis-light curve	$1.0\ 10^{-5}$	$gC\ m^2\ gCHL^{-1}$ $\mu molPhotons^{-1}$	
$c_{CHLC,max}$	Maximum algae CHL-to-C ratio	0.03	$gCHL\ gC^{-1}$	
$c_{CHLC,min}$	Minimum algae CHL-to-C ratio	0.002	$gCHL\ gC^{-1}$	
P^C_{max}	Maximum photosynthesis rate	$6.0\ 10^{-5}$	s^{-1}	
$k_{NO_{23}}$	NO_{23} half-saturation constant for algae growth	0.1	$mgN\ l^{-1}$	Bowie et al (1985), Chapra (1997)
k_{NH_4}	NH_4 half-saturation constant for algae growth	0.02	$mgN\ l^{-1}$	
k_{PO_4}	PO_4 half-saturation constant for algae growth	0.002	$mgP\ l^{-1}$	
k_{ew}	Light extinction due to particle-free water and color	0.05	m^{-1}	
s_{CHL1}	Algae self-shading factor	0.0088	$\mu gCHL^{-1}\ m^{-1}$	Chapra (1997), Riley (1956)
s_{CHL2}	Algae self-shading factor	0.054	$\mu gCHL^{-2/3}\ m^{-1}$	
s_{ISS}	ISS light shading factor	0.052	mgD^{-1}	Chapra (1997), Di Toro (1978)
s_{POM}	POM light shading factor	0.174	mgD^{-1}	
k_m	Algae mortality rate	$1.0\ 10^{-5}$	$kgN^{-1/3}\ s^{-1}$	Dunne et al (2005)
f^{PON}	Calibration factor of the terrestrial PON runoff	$2.7\ 10^{-3}$	unitless	Calibrated to match measurement-based river TKN estimates
$f_{m,DON}$	Fraction of algae mortality which is deposited to the DON pool	0.3	unitless	Bowie et al (1985); Calibrated to match measurement-based river nutrient

https://doi.org/10.5194/gmd-2022-236
Preprint. Discussion started: 2 January 2023

Geoscientific Model Development Discussions

$f_{m,PON}$	Fraction of algae mortality which is deposited to the PON pool	0.3	unitless	estimates
$f_{SedP,POP}$	Fraction of SedP resuspension which is deposited to the POP pool	0.9	unitless	
$f_{PON,DON}$	Fraction of PON decomposition which is deposited to DON pool	0.8	unitless	
$f_{POP,DOP}$	Fraction of POP decomposition which is deposited to DOP pool	0.8	unitless	
$f_{SedN,DON}$	Fraction of SedN decomposition which is deposited to DON pool	0.8	unitless	
$f_{SedP,DOP}$	Fraction of SedP decomposition which is deposited to DOP pool	0.8	unitless	
a	Reported fitted kinetic parameter in the PO_4 sorption/desorption	0.8	mgP gSS^{-1}	Garnier et al (2005)
b	Reported fitted kinetic parameter in the PO_4 sorption/desorption	0.2	unitless	
$k_{PO_4\_to\_PIP}$	Constant in the PO_4 sorption and desorption	0.5	unitless	Calibrated to match measurement-based river PO_4 estimates
$k_{SedN,d}$	SedN decomposition rate coefficient	0.001/sperd	s^{-1}	Bowie et al (1985); Calibrated to match measurement-based river nutrient estimates
$k_{SedP,d}$	SedP decomposition rate coefficient	0.001/sperd	s^{-1}	
$k_{PON,d}$	PON decomposition rate coefficient	0.001/sperd	s^{-1}	
$k_{POP,d}$	POP decomposition rate coefficient	0.001/sperd	s^{-1}	
$k_{DON,d}$	DON hydrolysis rate coefficient	0.2/sperd	s^{-1}	
$k_{DOP,d}$	DOP hydrolysis rate coefficient	0.01/sperd	s^{-1}	
k_{nitr}	Nitrification rate coefficient	0.4/sperd	s^{-1}	
k_{denitr}	Denitrification rate coefficient	0.3/sperd	s^{-1}	

Table 2: Model parameters, their descriptions, values, units, and references/rationale. "sperd" is seconds per days (86400).

https://doi.org/10.5194/gmd-2022-236
Preprint. Discussion started: 2 January 2023


Geoscientific Model Development Discussions

Once introduced from the land model to the river and lake systems, particulate solids and nutrients (i.e., SS, PON, and POP) are subject to either deposition or suspension based on a Rouse number-dependent criterion, defined as settling velocity divided by the von Karman constant and shear velocity (Pelletier, 2012).

$$R_{\#} = \frac{w_S}{\kappa \cdot u_*} = \frac{w_S}{\kappa\sqrt{g \cdot z \cdot S}}, \quad (4)$$

where $R_{\#}$ is Rouse number (unitless), w_S is settling velocity (m s^{-1}), κ is Karman constant (unitless), u_* is shear velocity (m s^{-1}), g is acceleration due to gravity (m s^{-2}), and z is river or lake depth (m). If Rouse number is less than 1.2 (a reported value in Pelletier, 2012), any newly introduced particulate matter, as well as those already in the bottom sediments (i.e., SedN, SedP, and Sed), are suspended into the water column and subject to transport through the river network. Otherwise, the particulate matter is deposited to the bottom sediments.

Settling velocity (w_s) is estimated as a function of grain diameter, fluid viscosity, and fluid and solid density (Ferguson and Church, 2004).

$$w_S = \frac{R \cdot g \cdot d^2}{C_2 \cdot \upsilon + (0.75 \cdot C_3 \cdot R \cdot g \cdot d^3)^{0.5}}, \quad (5)$$

where R is submerged specific gravity (unitless), d is particle diameter (m), υ is kinematic viscosity of the fluid (m^2 s^{-1}), and C_2 and C_3 are reported constants (unitless). For this initial FANSY implementation, a characteristic grain diameter (d) is assumed for all particulate material sinks.

For a batch river and lake system, a mass balance for SS and Sed is written as:

$$\frac{dSS}{dt} = \begin{cases} r_{DN} \cdot m(T) + \frac{Sed}{dt} & R_{\#} < 1.2 \\ r_{DN} \cdot m(T) - \frac{w_S}{z}\left(\frac{1}{dt} + \frac{w_S}{z}\right)^{-1} \frac{SS}{dt} & R_{\#} \geq 1.2 \end{cases}, \quad (6)$$

$$\frac{dSed}{dt} = \begin{cases} -\frac{Sed}{dt} & R_{\#} < 1.2 \\ \frac{w_S}{z}\left(\frac{1}{dt} + \frac{w_S}{z}\right)^{-1} \frac{SS}{dt} & R_{\#} \geq 1.2 \end{cases}, \quad (7)$$

where SS is suspended solid (kgD), Sed is benthic sediment (kgD), r_{DN} is algae D-to-N ratio (kgD kgN^{-1}), m(T) is temperature-dependent algae mortality (kgN s^{-1}), and z is river or lake depth (m). SS is gained by algae mortality (defined in Sect. 2.2.2) and benthic sediment (i.e., Sed) resuspension and lost by deposition. The opposite holds for Sed, except that Sed does not receive inputs from algae mortality. SS deposition is modeled by implicitly solving for the solid mass flux to Sed via w_S divided by a river or lake depth and multiplied by a solid mass in the water column. This implicit scheme reduces the numerical burden and improves stability.

https://doi.org/10.5194/gmd-2022-236
Preprint. Discussion started: 2 January 2023

Geoscientific Model Development Discussions

Given lack of knowledge of directly estimating organic contents from eroded soil, we divide SS into ISS and POM in rivers and lakes, based on an empirical nonlinear relationship showing that the fraction of particulate organic C (POC) in SS decreases with increasing SS concentration (Beusen et al., 2005; "log" referring to base 10). When input into Eq. (8), SS concentration is bounded to a numerically valid range of 0.009 to 2000 gD m^{-3}.

$$POC_{\%} = -0.160(\log[SS])^3 + 2.83(\log[SS])^2 - 13.6(\log[SS]) + 20.3\ , \quad (8)$$

$$[POM] = r_{DC} \cdot POC_{\%}/100 \cdot [SS]\ , \quad (9)$$

$$\begin{cases} [ISS] = [SS] - [POM] & \text{if } [SS] > [POM] \\ [ISS] = 0, [POM] = [SS] & \text{if } [SS] \le [POM] \end{cases}, \quad (10)$$

where [SS], [POM], and [ISS] are SS, POM, and ISS concentrations (gD m^{-3}), $POC_{\%}$ is POC content as % of SS, and r_{DC} is D-to-C ratio (kgD kgC^{-1}).

2.2.2 Algae dynamics

Algae dynamics are governed by net growth (i.e., gross growth – respiration) and a generalized mortality (i.e., non-predatory mortality + grazing + settling + excretion). For a batch river and lake system, a mass balance for algae is written as:

$$\frac{dNa}{dt} = \mu(I_{av}, T, N, P) \cdot Na - m(T)\ , \quad (11)$$

where Na is algae N (kgN) and $\mu(I_{av}, T, N, P)$ is algae net growth rate (s^{-1}) as a function of euphotic zone averaged irradiance I_{av}, T, N, and P.

A dynamic regulatory model was adapted to predict a CHL-to-C ratio (r_{CHLC}) and net growth rate (μ) as a function of euphotic zone averaged irradiance, temperature, and nutrients (Geider et al., 1997). The μ is the difference between photosynthesis and respiration rates, as represented in Eq. (12). The r_{CHLC} is up- and down-regulated in accordance with light and nutrient conditions according to Eq. (13).

$$\mu(I_{av}, T, N, P) = \frac{P_m^C}{1+\zeta} \cdot \left[1 - \exp\left(\frac{-\alpha^{CHL} \cdot I_{av} \cdot r_{CHLC}}{P_m^C}\right)\right], \quad (12)$$

$$r_{CHLC} = \max\left[r_{CHLC,min}, \frac{r_{CHLC,max}}{1+\left(\frac{r_{CHLC,max} \cdot \alpha^{CHL} \cdot I_{av}}{2 \cdot P_m^C}\right)}\right], \quad (13)$$

where P_m^C is C-specific, light-saturated photosynthesis rate (s^{-1}), ζ is cost of biosynthesis, α^{CHL} is CHL-specific initial slope of the photosynthesis-light curve (gC m^2 $gCHL^{-1}$ μmolPhotons^{-1}), I_{av} is euphotic zone averaged irradiance (μmolPhotons m^{-2} s^{-1}), r_{CHLC} is algae CHL-to-C ratio (kgCHL kgC^{-1}), and $r_{CHLC,min}$ and $r_{CHLC,max}$ are minimum and maximum algae CHL-to-C ratios (kgCHL kgC^{-1}).

https://doi.org/10.5194/gmd-2022-236
Preprint. Discussion started: 2 January 2023


Geoscientific Model Development Discussions

The C-specific, light-saturated photosynthesis rate (P_m^C) is calculated as a function of temperature and nutrient limitation, also following the approach of Geider et al. (1997).

$$P_m^C(T,N) = P_{max}^C(T) \cdot \min\left[\left(\lim_{NO_{23}} + \lim_{NH_4}\right), \lim_{PO_4}\right], \quad (14)$$

where $P_{max}^C(T)$ is temperature-dependent maximum photosynthesis rate (s^{-1}), $\lim_{NO_{23}}$, $\lim_{NH_4}$, and $\lim_{PO_4}$ are NO_{23}, NH_4, and PO_4 limitations (unitless).

In LM3-FANSY, freshwater biogeochemical reaction rates approximately double for a temperature increase of 10°C based on the Arrhenius equation, with a scaling factor θ based on Eppley (1972). The simulated maximum and minimum water temperatures were limited to 30°C and -3°C respectively.

$$P_{max}^C(T) = P_{max}^C \cdot \theta^{T-T_{ref}}, \quad (15)$$

where T is temperature (°C), T_{ref} is reference temperature (°C), P_{max}^C is maximum photosynthesis rate at T_{ref} (s^{-1}), and θ is empirical temperature correction factor.

To combine the limiting effects of nutrients N and P, Liebig's law of the minimum is used. A NH_4 preference factor is used to account for inhibition of NO_{23} uptake when NH_4 concentrations are high compared to a NH_4 half-saturation constant (Frost and Franzen, 1992). A saturating Monod relationship is used for handling the NH_4 and PO_4 limiting effects. The maximum NO_{23}, NH_4, and PO_4 concentrations were limited to 10 moles l^{-1} to avoid numerically rare behavior under extremely dry conditions.

$$\lim_{NO_{23}} = \frac{[NO_{23}]}{(k_{NO_{23}}+[NO_{23}]) \cdot (1+\frac{[NH_4]}{k_{NH_4}})}, \quad (16)$$

$$\lim_{NH_4} = \frac{[NH_4]}{k_{NH_4}+[NH_4]}, \quad (17)$$

$$\lim_{PO_4} = \frac{[PO_4]}{k_{PO_4}+[PO_4]}, \quad (18)$$

where $[NO_{23}]$, $[NH_4]$, and $[PO_4]$ are NO_{23}, NH_4, and PO_4 concentrations ($gN\ m^{-3}$) and $k_{NO_{23}}$, k_{NH_4}, and k_{PO_4} are NO_{23}, NH_4, and PO_4 half-saturation constants for algae growth ($gN\ m^{-3}$).

Photosynthetically available, visible irradiance at the surface is used for algae growth dynamics. Light attenuation with depth is modeled by the Beer-Lambert law using an extinction coefficient (k_e, Chapra, 1997). The euphotic zone (depth where light intensity falls to one percent of that at the surface) averaged light level (I_{av}) is used. The extinction coefficient is estimated

https://doi.org/10.5194/gmd-2022-236
Preprint. Discussion started: 2 January 2023


Geoscientific Model Development Discussions

dynamically to account for temporal variations in turbidity due to algae shading (Riley, 1956), light extinction due to particle-free water and color, and variations in nonvolatile ISS and POM (Dio Toro, 1978).

$$I_z = I_s \cdot e^{-k_e z}\,, \tag{19}$$

$$z_{0.01} = -\frac{\ln(0.01)}{k_e}\,, \tag{20}$$

$$I_{av} = \begin{cases} \frac{I_s}{k_e \cdot z}\left(1 - e^{-k_e \cdot z}\right) & z \le z_{0.01} \\ \frac{I_s}{k_e \cdot z_{0.01}}\left(1 - e^{-k_e \cdot z_{0.01}}\right) & z > z_{0.01} \end{cases}, \tag{21}$$

$$k_e = k_{ew} + s_{ISS} \cdot [ISS] + s_{POM} \cdot [POM] + s_{CHL1} \cdot [CHL] + s_{CHL2} \cdot [CHL]^{2/3}\,, \tag{22}$$

where I_z and I_s are irradiance at z and at the surface (µmolPhotons m^{-2} s^{-1}), $z_{0.01}$ is river or lake depth where light intensity falls to one percent of that at the surface (m), k_e is light extinction coefficient (m^{-1}), k_{ew} is light extinction due to particle-free water and color (m^{-1}), s_{CHL1} and s_{CHL2} are algae self-shading factors (µgCHL^{-1} m^{-1} and µg$CHL^{-2/3}$ m^{-1}), s_{ISS} and s_{POM} are constants accounting for the impacts of ISS and POM (m^3 gD^{-1} m^{-1}), and [CHL] is CHL concentration (µgCHL l^{-1}).

Biomass-specific algal mortality is assumed to increase non-linearly with algae concentration, reflecting a presumed increase in predators with algal prey (e.g., Steele and Henderson, 1992).

$$m(T) = k_m(T) \cdot Na^{4/3}\,, \tag{23}$$

where k_m is temperature-dependent algae mortality rate (kg$N^{-1/3}$ s^{-1}). Exponents between 4/3 and 2 have been commonly applied in this relationship, with higher values corresponding to more tightly coupled top-down control (Dunne et al., 2005). We have adopted a value of 4/3 to enable high biomass in nutrient rich environments. An Arrhenius relationship with the same scaling as phytoplankton growth is applied to account for the effect of temperature on grazing (Eq. 15). The division of algal mortality between inorganic/organic and dissolved/particulate nutrient pools is described in the following sections.

Algae D, P, C, and CHL are diagnosed from algae N using corresponding stoichiometric ratios (Chapra, 1997) and r_{CHLC} estimated above based on Geider et al. (1997).

$$Da = Na \cdot r_{DN}\,, \tag{24}$$

$$Pa = Na \cdot r_{PN}\,, \tag{25}$$

$$Ca = Na \cdot r_{CN}, \tag{26}$$

$$CHL = Ca \cdot r_{CHLC}, \tag{27}$$

https://doi.org/10.5194/gmd-2022-236
Preprint. Discussion started: 2 January 2023


Geoscientific Model Development Discussions

where Da, Pa, Ca, and CHL are algae D (kgD), P (kgP), C (kgC), and CHL (kgCHL) and r_{DN}, r_{PN}, r_{CN}, and r_{CHLC} are algae D-to-N (kgD kgN^{-1}), P-to-N (kgP kgN^{-1}), C-to-N (kgC kgN^{-1}), and CHL-to-C (kgCHL kgC^{-1}) ratios.

2.2.3 N dynamics

In LM3-FANSY, PON runoff is estimated as the product of a fast and slow litter N concentration and water drainage from active soil layer. The concentration is calculated as dividing N contents in fast and slow litter pools by an effective soil depth, which is approximated assuming C weight content 3.4% and average soil density 1500 kg m^{-3}(Gerber et al., 2010). While land model physics represents vertically distributed soil–water, soil–ice, and temperature profiles, with thinnest layer of 0.02 m near the surface to many meters below the surface (Milly et al., 2014), soil C-N model is vertically lumped. Thus, N runoff from the lumped single-layer N pools based on the average water drainage bypasses most of the vertically distributed soil hydrologic system (Lee et al., 2014). The calibration factor, f^{PON}, is used to slow overall N movement from the litter pools to rivers, in addition to compensate reductions due to hydraulic controls that are not accounted for in the model (e.g., dams, reservoirs). This calibration factor is fit to match measurement-based river Total Kjeldahl method N (TKN, the sum of NH_4, DON, and PON) estimates, due to limited measurement-based PON estimates.

$$R^{PON} = f^{PON} \cdot \frac{D_s}{\rho_w} \cdot [N_{PON}] = f^{PON} \cdot \frac{D_s}{\rho_w} \cdot \left(\frac{N_{FL}+N_{SL}}{h_s}\right), \quad (28)$$

where R^{PON} is PON runoff from litter pools to rivers (kgN m^{-2} s^{-1}), D_s is water drainage from active soil layer (kg m^{-2} s^{-1}), f^{PON} is calibration factor (unitless), $[N_{PON}]$ is fast and slow litter N concentration (kgN m^{-3}), h_s is effective soil depth (m), and N_{FL} and N_{SL} are N contents in fast and slow litter pools (kgN m^{-2}).

For a batch river and lake system, a mass balance is written for PON and SedN as:

$$\frac{dPON}{dt} = \begin{cases} f_{m,PON} \cdot m(T) - k_{PON,d}(T) \cdot PON + \frac{SedN}{dt} & R_{\#} < 1.2 \\ f_{m,PON} \cdot m(T) - k_{PON,d}(T) \cdot PON - \frac{w_S}{z}\left(\frac{1}{dt} + \frac{w_S}{z}\right)^{-1} \frac{PON}{dt} & R_{\#} \geq 1.2 \end{cases}, \quad (29)$$

$$\frac{dSedN}{dt} = \begin{cases} -k_{SedN,d}(T) \cdot SedN - \frac{SedN}{dt} & R_{\#} < 1.2 \\ -k_{SedN,d}(T) \cdot SedN + \frac{w_S}{z}\left(\frac{1}{dt} + \frac{w_S}{z}\right)^{-1} \frac{PON}{dt} & R_{\#} \geq 1.2 \end{cases}, \quad (30)$$

where PON is particulate organic N (kgN), SedN is sediment N (kgN), $f_{m,PON}$ is fraction of algae mortality which is deposited to the PON pool (unitless), $k_{PON,d}(T)$ and $k_{SedN,d}(T)$ are temperature-dependent PON and SedN decomposition rates (s^{-1}). FANSY PON is gained by algae mortality and benthic sediment (i.e., SedN) resuspension and lost by deposition and decomposition. The same holds for SedN, except that it does not receive inputs from algae mortality. A fraction ($f_{m,PON}$) is introduced to represent the portion of algae mortality released as PON. First-order kinetics are used to describe various decay processes and transformations, with the Arrhenius-based relationship to adjust rate coefficients for temperature effects

https://doi.org/10.5194/gmd-2022-236
Preprint. Discussion started: 2 January 2023


Geoscientific Model Development Discussions

(Eq. 15). PON and SedN are lost by decay processes that breakdown complex organic compounds into simpler organic N (i.e., DON) or into NH_4. Rate coefficients for these decay processes are thus much smaller than those for release of NH_4 due to DON decay processes (i.e., hydrolysis), oxidation of NH_4 to NO_{23} (i.e., nitrification), and reduction of NO_{23} to N_2 (i.e., denitrification) (Table 2; Chapra, 2008).

FANSY DON is gained by algae mortality and decomposition of PON and SedN and lost by hydrolysis. A fraction ($f_{m,DON}$) is introduced to represent the portion of algae mortality released as DON. Decomposition of PON and SedN releases both dissolved organic and inorganic N (i.e., DON and NH_4). Fractions ($f_{PON,DON}$ and $f_{SedN,DON}$) are introduced to divide the proportions between DON and NH_4.

$$\frac{dDON}{dt} = f_{m,DON} \cdot m(T) + f_{PON,DON} \cdot k_{PON,d}(T) \cdot PON + f_{SedN,DON} \cdot k_{SedN,d}(T) \cdot SedN - k_{DON,d}(T) \cdot DON, \quad (31)$$

where DON is dissolved organic N (kgN), $f_{m,DON}$ is the fraction of algae mortality which is deposited to the DON pool (unitless), $f_{PON,DON}$ and $f_{SedN,DON}$ are the fractions of PON and SedN decomposition which are deposited to the DON pool (unitless), and $k_{DON,d}(T)$ is temperature-dependent DON hydrolysis rate (s^{-1}).

FANSY NH_4 and NO_{23} are removed by algae uptake during photosynthesis. NH_4 is returned to the water column through soluble excretions of algae (which is included in the algae mortality term) and decomposition/hydrolysis of SedN, PON, and DON. Removal of NH_4 by nitrification generates NO_{23}, which is in turn lost by denitrification.

$$\frac{dNH_4}{dt} = \left(1 - f_{m,PON} - f_{m,DON}\right) \cdot m(T) + \left(1 - f_{PON,DON}\right) \cdot k_{PON,d}(T) \cdot PON + \left(1 - f_{SedN,DON}\right) \cdot k_{SedN,d}(T) \cdot SedN + k_{DON,d}(T) \cdot DON - k_{nitr}(T) \cdot NH_4 - f_{NH_4,up}\mu(I_{av}, T, N, P) \cdot Na, \quad (32)$$

$$\frac{dNO_{23}}{dt} = k_{nitr}(T) \cdot NH_4 - k_{denitr}(T) \cdot NO_{23} - (1 - f_{NH_4,up}) \cdot \mu(I_{av}, T, N, P) \cdot Na, \quad (33)$$

$$f_{NH_4,up} = \left(\frac{lim_{NH_4}}{lim_{NO_{23}} + lim_{NH_4}}\right), \quad (34)$$

where NH_4 and NO_{23} are ammonium and nitrite plus nitrate N (kgN), $k_{nit}(T)$ and $k_{denit}(T)$ are temperature-dependent nitrification and denitrification rates (s^{-1}), and $f_{NH_4,up}$ is the fraction of NH_4 uptake for algae growth (unitless).

2.2.4 P dynamics

Overall, P dynamics are similar to those of N, but with several differences. Because there are two suspended forms of POP and PIP, SedP resuspension is divided into POP and PIP pools with a fraction of $f_{SedP,POP}$. Unlike N, P does not exist in a gaseous form, and FANSY includes no loss term for P to the atmosphere. Dissolved inorganic P sorbs strongly to solid

https://doi.org/10.5194/gmd-2022-236
Preprint. Discussion started: 2 January 2023

Geoscientific Model Development Discussions

particles. The exchange of PO_4 between the dissolved and particulate forms are modeled based on Freundlich kinetics (Garnier et al., 2005; Nemery, 2003), with the flux proportional to the disequilibrium between the two phases.

$$\frac{dPOP}{dt} = \begin{cases} c_{PN} \cdot f_{m,PON} \cdot m(T) - k_{POP,d}(T) \cdot POP + f_{SedP,POP} \cdot \frac{SedP}{dt} & R_{\#} < 1.2 \\ c_{PN} \cdot f_{m,PON} \cdot m(T) - k_{POP,d}(T) \cdot POP - \frac{w_S}{z}\left(\frac{1}{dt} + \frac{w_S}{z}\right)^{-1} \frac{POP}{dt} & R_{\#} \geq 1.2 \end{cases}, \quad (35)$$

$$\frac{dSedP}{dt} = \begin{cases} -k_{SedP,d}(T) \cdot SedP - \frac{SedP}{dt} & R_{\#} < 1.2 \\ -k_{SedP,d}(T) \cdot SedP + \frac{w_S}{z}\left(\frac{1}{dt} + \frac{w_S}{z}\right)^{-1} \left(\frac{dPOP}{dt} + \frac{PIP}{dt}\right) & R_{\#} \geq 1.2 \end{cases}, \quad (36)$$

$$\frac{dPIP}{dt} = \begin{cases} F_{PO_4\_to\_PIP} + \left(1 - f_{SedP,POP}\right)\frac{SedP}{dt} & R_{\#} < 1.2 \\ F_{PO_4\_to\_PIP} - \frac{w_S}{z}\left(\frac{1}{dt} + \frac{w_S}{z}\right)^{-1} \frac{dPIP}{dt} & R_{\#} \geq 1.2 \end{cases}, \quad (37)$$

$$\frac{dDOP}{dt} = c_{PN} \cdot f_{m,DON} \cdot m(T) + f_{POP,DOP} \cdot k_{POP,d}(T) \cdot POP + f_{SedP,DOP} \cdot k_{SedP,d}(T) \cdot SedP - k_{DOP,d}(T) \cdot DOP, \quad (38)$$

$$\frac{dPO_4}{dt} = c_{PN} \cdot \left(1 - f_{m,PON} - f_{m,DON}\right) \cdot m(T) + \left(1 - f_{POP,DOP}\right) \cdot k_{POP,d}(T) \cdot POP + \left(1 - f_{SedP,DOP}\right) \cdot k_{SedP,d}(T) \cdot SedP + k_{DOP,d}(T) \cdot DOP - c_{PN} \cdot \mu(I_{av}, T, N, P)Na - F_{PO_4\_to\_PIP}, \quad (39)$$

$$[PIP_{eq}] = a \cdot [PO_4]^b \cdot [ISS]_2, \quad (40)$$

$$F_{PO_4\_to\_PIP} = k_{PO_4\_to\_PIP} \cdot ([PIP_{eq}] - [PIP]) \cdot H_2O \cdot 10^{-3}, \quad (41)$$

where POP is particulate organic P (kgP), SedP is sediment P (kgP), PIP is particulate inorganic P (kgP), DOP is dissolved organic P (kgP), PO_4 is phosphate (kgP), H_2O is water volume (m^3), $k_{POP,d}(T)$ and $k_{SedP,d}(T)$ are temperature-dependent POP and SedP decomposition rates (s^{-1}), $k_{DOP,d}(T)$ is temperature-dependent DOP hydrolysis rate (s^{-1}), $f_{SedP,POP}$ is the fraction of SedP resuspension which is deposited to the POP pool (unitless), $f_{POP,DOP}$ and $f_{SedP,DOP}$ are the fractions of POP and SedP decomposition which are deposited to the DOP pool (unitless), [PIP] and [PO_4] are PIP and PO_4 concentrations (mgP l^{-1}), $[ISS]_2$ is ISS concentration (gD l^{-1}) (Notice the concentration unit difference from [ISS] in Eq. 10), $[PIP_{eq}]$ is PIP equilibrium concentration (mgP l^{-1}), $F_{PO_4\_to\_PIP}$ is fluxes from PO_4 to PIP (kgP), $k_{PO_4\_to\_PIP}$ is a constant controlling the equilibration of sorbed PO_4 to inorganic sediments (unitless), and a (mgP gSS^{-1}) and b (unitless) are reported empirical kinetic parameters.

3 Model forcing and simulations

3.1 Baseline simulations

LM3-FANCY was implemented globally at 1 degree spatial and 30 minute temporal resolution with all inputs regridded to 1 degree resolution. Following ~11,000 years of spin-up from Lee et al. (2019), the terrestrial component LM3 was run for the

https://doi.org/10.5194/gmd-2022-236
Preprint. Discussion started: 2 January 2023


Geoscientific Model Development Discussions

period 1700-1899 by recycling 30 years (1948-1977) of observation-based, historical climate forcing (Sheffield et al., 2006) and Coupled Model Intercomparison Project (CMIP6) datasets for atmospheric CO_2 (Meinshausen et al., 2017), atmospheric N deposition (CMIP6 Forcing Datasets Summary), and land-use states and transitions (Hurtt et al., 2020). Since the freshwater component requires a shorter time for equilibrium than vegetation and soil, the merged terrestrial and freshwater components LM3-FANSY were run for only the 1900-2010 period using additional CMIP6 datasets for fertilizer N applications (Hurtt et al., 2020) and reported point and nonpoint N and P inputs to rivers (Beusen et al., 2015). Here we calibrate the model parameters (Table 2) based on contemporary year 1990's results and limit our focus to a period (1982-2010), providing a global cross-watershed perspective of contemporary sediment and nutrient loadings for comparison with observation-based estimates. Analyses of the past periods and interannual/seasonal variability are left to future work.

The observation-based, historical climate forcing data available for the period 1948-2010 (Sheffield et al., 2006) includes precipitation, specific humidity, air temperature, surface pressure, wind speed, and short- and long-wave downward radiation at 1 degree and 3 hour resolution. This forcing was cycled over a period of 30 years (1948–1977) to perform long-term simulations from 1700 to 1947, and the 1948–2010 forcing data were used for the simulations from 1948 to 2010. The annual atmospheric CO_2 (Meinshausen et al., 2017) available for the period 1-2500 is used for the corresponding period simulation from 1700 to 2010. The atmospheric N deposition data (CMIP6 Forcing Datasets Summary) includes two forms of oxidized and reduced N (NO_y and NH_x) at 2.5 longitude by 1.9 latitude degree and 1 month resolution for the period 1850-2099. The NO_y and NH_x deposition for the year 1850 was applied to soil NO_{23} and NH_4 pools respectively for the 1700-1849 simulation, and then the 1850-2010 deposition was applied for the 1850-2010 simulation.

The dataset of land-use states and transitions and fertilizer N applications at 0.25 degree and 1 year resolution (Hurtt et al., 2020) is available for the period 850-2100. The 1700-2010 land-use state and transition data is used for the simulations from 1700 to 2010. Since the amount of fertilizer applications in the dataset is zero until 1915, the 1916-2010 fertilizer N was applied for the simulations from 1916 to 2010. For land use and fertilizer applications, 12 land-use types reported in the Land Use Harmonization (LUH2) (Hurtt et al., 2020) were grouped into 4 types in LM3-FANSY: 1) primary land in LM3-FANSY is the sum of forested primary land and non-forested primary land in LUH2, 2) secondary land in LM3-FANSY is the sum of potentially forested secondary land, potentially non-forested secondary land, and urban land in LUH2, 3) cropland in LM3-FANSY is the sum of C3 annual cropland, C3 perennial cropland, C4 annual cropland, C4 perennial cropland, and C3 N-fixing cropland in LUH2, and 4) pasture in LM3-FANSY is the sum of managed pasture and rangeland in LUH2. The sum of fertilizers allocated to the 5 croplands in LUH2 was applied to the cropland in LM3-FANSY.

The terrestrial soil detachment component requires slope, rainfall, and LAI as inputs. Rainfall was simulated by using 3 hourly precipitation and temperature from Sheffield et al. (2006) and assuming that all of the precipitation falls as snow with the temperature less than 0°C, otherwise it is assumed to be rain. We used slope data derived from Danielson and Gesch

https://doi.org/10.5194/gmd-2022-236
Preprint. Discussion started: 2 January 2023


Geoscientific Model Development Discussions

(2011). We used an observationally derived, monthly average global vegetation LAI dataset from Global Inventory Modeling and Mapping Studies (GIMMS) Normalized Difference Vegetation Index (NDVI3g) for the period 1982-2010 (Zhu et al., 2013) to avoid potential errors that might be caused by using modeled LAI. The 1982 LAI was used to perform long-term simulation from 1900 to 1981 and the 1982-2010 LAI was used for the simulations from 1982 to 2010.

Solids and nutrient inputs from terrestrial systems and the atmosphere to rivers are simulated by LM3-FANSY or provided by Beusen et al. (2015) (Table 3). We divided yearly total N (TN) and total P (TP) inputs from Beusen et al. (2015) into different N and P forms based on Vilmin et al. (2018). Organic N (ON) and organic P (OP) from Beusen et al. (2015) were considered to be mainly (70%) particulate.

	N			P			Solid	
	NH_4	NO_{23}	ON	PO_4	PIP	OP	POM	ISS
Litter from floodplains	LM3-FANCY	LM3-FANCY	LM3-FANCY	0.00	0.00	1.00	LM3-FANCY	LM3-FANCY
Agricultural surface runoff				0.34	0.33	0.33		
Natural land surface runoff				0.00	0.25	0.75		
Subsurface runoff								
Aquaculture	0.26	0.62	0.12	0.69	0.06	0.25		
Wastewater	0.90	0.00	0.10	0.80	0.10	0.10		
Atmospheric deposition	0.35	0.35	0.30					
Weathering				1.00	0.00	0.00		

Table 3: Description of solid and nutrient inputs from terrestrial systems and the atmosphere to rivers, which were simulated by LM3-FANSY or provided by Beusen et al. (2015). The numbers are the fractions of dividing TN and TP provided by Beusen et al. (2015) into different species based on Vilmin et al. (2018).

3.2 Sensitivity simulations

Model sensitivities to components, parameters, and inputs are examined by changing those values and examining the responses of global river solid and nutrient loads and changes in Pearson correlation coefficients (r) between measurement-based and modeled estimates across world major rivers. A small contribution of the component, parameter, or input to global loads and/or regional variations (as represented by r values) implies its little impact on modeling skill. The opposite holds for that with a large impact.

Model sensitivities to the one free terrestrial soil detachment parameter (C_1) are analyzed by changing the value by ±15%. Model sensitivities to N runoff from LM3-FANSY and to nutrient input datasets from Beusen et al (2015) (Table 3) are examined by increasing each model input source by 15% and by removing each input source. One of the distinct features of LM3-FANSY is the capability of modeling interactions of algae and nutrient dynamics with solid dynamics. We use light

https://doi.org/10.5194/gmd-2022-236
Preprint. Discussion started: 2 January 2023


Geoscientific Model Development Discussions

shading by SS and algae themselves to modulate the strength of algal productivity and examine the sensitivity of riverine outputs to more/less active algal populations. In LM3-FANSY, a light extinction coefficient is dynamically simulated as a function of ISS, POM, and CHL (Eq. 22), instead of using a prescribed parameter. To evaluate how critical the dynamic light extinction component is for modeling capacity, the component was replaced with prescribed parameter values (k_e = 0.15 and 0.45) and the responses are examined. Another process that has not been resolved in previous global models is the interactions of PO_4 sorption/desorption with solid particles. As described in Section 2.2.4, LM3-FANSY adopted a Freundlich kinetics approach (Garnier et al., 2005; Nemery, 2003) to model the exchange of PO_4 between the dissolved and particulate forms. The sensitivity to the reported two empirical parameters (a and b from Eq. 40) is analyzed by changing the values by ±15%. Finally, unlike P, the N cycle includes an additional loss pathway to the atmosphere via denitrification. The role of denitrification on global loads and/or regional variations, however, has not been investigated by previous global watershed models. Model sensitivities to denitrification are analyzed by changing the first order denitrification rate coefficient value by ±15%.

3.3 Comparisons of measurement-based and modeled estimates

We compare LM3-FANSY results of river SS, NO_{23}, NH_4, DON, TKN, PO_4, DOP, and TP (the sum of PO_4, DOP, PIP, and POP) yields (kg km^{-2} yr^{-1}), loads (kt yr^{-1}), and concentrations (mg l^{-1}) with measurement-based estimates for 69 of the world's major rivers (Meybeck and Ragu, 2012), which are distributed globally and influenced by various climates and land use (Table SI1-9). River basins with area < 100,000 km^2, about 10 grid cells in our 1 degree resolution, are excluded from the comparison. Since hydraulic controls like damming, irrigation, and diversion affect many rivers, Meybeck and Ragu (2012) distinguish natural river discharges from actual, modified ones. LM3-FANSY does not resolve such hydraulic controls and thus, if available, the natural discharges of Meybeck and Ragu (2012) are used, when calculating loads and yields from their multi-year average concentrations. We also report prediction errors computed as the difference between the modeled and measurement-based estimates of loads expressed as a percentage of the measurement-based loads. We analyze simulations between 1982-2010 and note that the Meybeck and Ragu (2012) estimates, mostly reported between 1970s-1990s, do not necessarily match the target period in this study. Cross-watershed contrasts are thus the primary target of our comparisons, not contemporary fluctuations and trends.

4 Results and discussion

4.1 Model performance analysis

Measurement-based and simulated SS estimates across 64 rivers are significantly correlated, with Pearson correlation coefficient, r values equal to 0.66 for yields, 0.77 for loads, and 0.67 for concentrations for the year 1990 (Fig. 2, Table 4). This result, corresponding to a coarsely calibrated value of the one free terrestrial soil detachment parameter (C_1=0.015), demonstrates that LM3-FANSY reproduces the measurement-based SS estimates well, especially given that the model

https://doi.org/10.5194/gmd-2022-236
Preprint. Discussion started: 2 January 2023

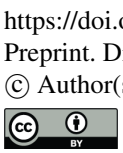

Geoscientific Model Development Discussions

contains only one calibrated parameter for SS. This model performance is competitive with other global model estimates using larger numbers of free parameters (Hatono and Yoshimura, 2020; Mayorga et al., 2010; Pelletier, 2012; Tan et al., 2017). For example, model performance of Global NEWS 2, when analyzed on the same dataset used for our model performance evaluation, yet excluding a few unavailable rivers (Table SI1), is slightly better than LM3-FANSY for yields and loads and slightly worse for concentrations based on correlations (Fig SI1). The total amount of global river SS loads to the coastal ocean estimated as 9-11 Pg yr^{-1} between 1982-2010 by LM3-FANSY (Table 5) is at the lower bond of previous estimates (Table 6, Global NEWS estimates of 11-27 Pg yr^{-1}, Beusen et al., 2005; Discharge Relief Temperature sediment delivery model (QRT) estimate of 13 Pg yr^{-1}, Syvitski et al., 2005).

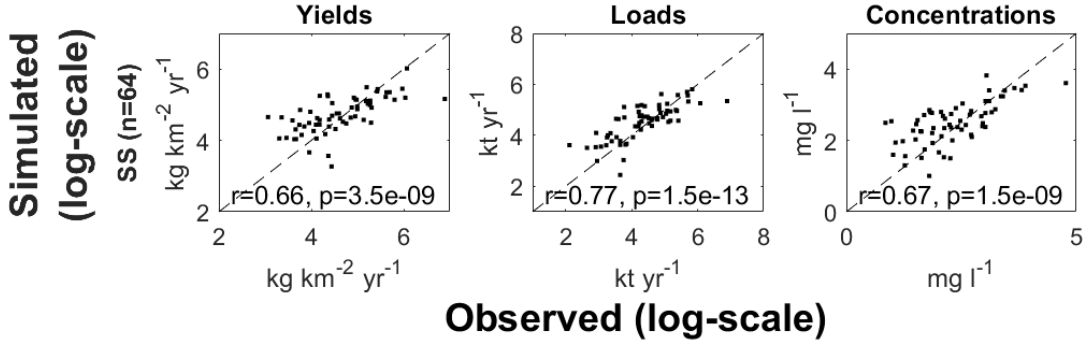

Figure 2: Pearson correlation coefficients (r) and p values (p) between measurement-based vs. simulated SS yields, loads, and concentrations across 64 rivers for the year 1990.

Input/parameter changes or prediction errors		SS	NO_{23}	NH_4	DON	TKN	PO4	DOP	TP
B	-	.77 (.71-.77)	.78 (.75-.81)	.67 (.62-.77)	.84 (.84-.94)	.77 (.71-.87)	.72 (.67-.73)	.95 (.94-.96)	.98 (.95-.99)
+15%	N & P in aquaculture	-	-2	-1	-	-5	-5	-2	-
+15%	N in atmos. deposition	-	1	-	-	-	-	-	-
+15%	N & P in wastewater	-	1	-	-	-	-	-	-
+15%	P in weathering	-	1	-	-	-	-	-	-
+15%	N & P in soil runoff	-	1	-	-	-	-	-	-
+15%	N & P in litter runoff	-	-	-1	-	-1	-	-	-1
R	N & P in aquaculture	-	1	-	-	-	-2	-	-
R	N in atmos. deposition	-	1	-	-	-	-	-	-

https://doi.org/10.5194/gmd-2022-236
Preprint. Discussion started: 2 January 2023

Geoscientific Model Development Discussions

R	N & P in wastewater	-	-	-	-	-1	-1	1	-
R	P in weathering	-1	-	-11	-	-	-4	-	-2
R	N & P in runoff	-1	1	-	-	-	-6	-	-4
R	N & P in litter runoff	-	-13	-31	-56	-1	-17	-8	-3
R	Dynamic light extinction coefficient (k_e=0.15, 0.45)	-2, -2	1, -3	-, -2	-	-14, -5	-1, -8	-1, -2	-4, -
±15%	Free parameter of terrestrial soil detachment (C_1=0.017, 0.013)	-	1, 1	-	-	-	-, -2	-	-
±15%	PO4 sorption/desorption parameter (a=0.92, 0.68)	-	1, 1	-	-	-	1, -1	-	-
±15%	PO4 sorption/desorption parameter (b=0.23, 0.17)	-	1, 1	-	-	-	0, 1	-	-
±15%	Denitrification rate coefficient (k_{denitr}=0.35, 0.23)	-	1, -	-	-	-	-	-	-

Table 4: Pearson correlation coefficients (r) between measurement-based vs. simulated loads across world major rivers for the year 1990 (between 1982-2010 in parenthesis) in the baseline (noted as "B" in this table) and sensitivity simulations. Model sensitivity to components, parameters, and inputs was examined by removing ("R") or changing ("+15%" or "±15%") each of them and examining the responses in model outputs by recalculating r values and examining their percentage (%) differences from the baseline simulation. Dashes indicate no changes.

	Input or parameter	Global river loads to the coastal ocean								
		SS	TN	DIN	DON	PON	TP	DIP	DOP	PP
B	-	9262-10907 (9977)	36.4-41.3 (38.9)	10.6-12.2 (11.5)	12.0-13.8 (13.0)	12.9-15.7 (14.3)	6.5-7.8 (7.3)	1.9-2.7 (2.4)	0.6-0.7 (0.7)	3.9-4.5 (4.2)
+15%	N & P in aquaculture	-	-	-	-	-	-	-	-	-
+15%	N in atmos. deposition	-	-	-	-	-	-	-	-	-
+15%	N & P in wastewater	-	1	2	-	1	2	3	1	1
+15%	P in weathering	-	-	-	-	-	2	5	-	1
+15%	N & P in soil runoff	-	9	12	15	1	9	12	10	8
+15%	N & P in litter runoff	-	5	-	-	13	2	-	5	2
R	N & P in aquaculture	-	-	-1	-	-	-1	-1	-1	-
R	N in atmos. deposition	-	-	-	-	-1	-	-	-	-
R	N & P in wastewater	-	-7	-16	-1	-4	-10	-17	-6	-7

https://doi.org/10.5194/gmd-2022-236
Preprint. Discussion started: 2 January 2023

Geoscientific Model Development Discussions

R	P in weathering	-	-1	-	-	-2	-14	-28	-4	-7
R	N & P in runoff	-	-60	-82	-99	-6	-63	-63	-65	-62
R	N & P in litter runoff	-	-33	-	-	-90	-12	-2	-31	-15
R	Dynamic light extinction coefficient (k_e=0.15-0.45)	4, 4	18, 16	-9, -7	6, 5	45, 39	-	-40, -33	93, 78	4, 4
±15%	Free parameter of terrestrial soil detachment (C_1=0.017, 0.013)	13, -13	-	-	-	-	-	-4, 5	-	2, -3
±15%	PO4 sorption/desorption parameter (a=0.92, 0.68)	-	-	-	-	-	-	-6, 7	-	3, -4
±15%	PO4 sorption/desorption parameter (b=0.23, 0.17)	-	-	-	-	-	-	2, -3	-	-1, 1
±15%	Denitrification rate coefficient (k_{denitr}=0.35, 0.23)	-	-2, 3	-5, 11	-	-, 1	-	-, -1	-1, 1	-
Min	Prediction errors	-97	-90	-74	-72	-32	-87	-59	-64	Min
25th	Prediction errors	-32	-24	-40	-43	44	-39	-27	-63	25th
Med	Prediction errors	40	56	26	23	97	17	10	-9	Med
75th	Prediction errors	270	345	544	231	394	181	66	80	75th
Max	Prediction errors	3062	1186	3114	573	671	5539	317	182	Max
IQR	Prediction errors	302	369	584	274	350	221	93	143	IQR

Table 5: Global river loads (Tg yr^{-1}) to the coastal ocean in the baseline simulation (noted as "B" in this table) between 1982-2010 (1982-2010 mean values in parentheses). Model sensitivity to components, parameters, and inputs was examined by removing ("R") or changing ("+15%" or "±15%") each of them and examining the responses in model outputs by calculating percentage (%) differences in river loads between the baseline and sensitivity simulations. Dashes indicate no changes. Prediction errors are computed as the difference between the simulated and measurement-based estimates of loads expressed as a percentage of the measurement-based loads.

	Pg yr^{-1}	Tg yr^{-1}							
	SS	TN	DIN	DON	PON	TP	DIP	DOP	PP
Global NEWS	19 (11-27, Beusen et al	44.9 (NEWS 2; Mayorga	18.9 (NEWS 2; Mayorga	10 (NEWS-DON; Harrison	13.5 (NEWS 2; Mayorga	9.0 (NEWS 2; Mayorga	1.45 (NEWS-DIP-HD; Harrison	0.6 (NEWS-DOP; Harrison	6.6 (NEWS 2; Mayorga

https://doi.org/10.5194/gmd-2022-236
Preprint. Discussion started: 2 January 2023


Geoscientific Model Development Discussions

	2005)	et al., 2010)	et al., 2010)	et al., 2005)	et al., 2010)	et al., 2010)	et al., 2010)	et al., 2005)	et al., 2010)
QRT; Syvitski et al (2005)	13								
IMAGE-GNM; Beusen et al (2016)		36.5				4			
Boyer et al., 2006		48							
Galloway et al., 2004		47.8							
Green et al., 2004		40	14.5						
Smith et al., 2003			18.9				2.3		

Table 6: Published estimates of global river loads to the coastal ocean.

480 Correlations between measurement-based vs. simulated NO_{23}, NH_4, DON, and TKN yields, loads, and concentrations across 50, 36, 18, and 11 rivers respectively (Fig. 3, Table 4) indicate that LM3-FANSY can also explain the observed spatial variations in river N in multiple forms and units to a reasonable extent. The modeling capacity of LM3-FANSY in terms of N is comparable to that of Global NEWS 2 (which does not estimate NO_{23} and NH_4 separately, but only estimate their sum as DIN). Spatial DIN patterns evaluated by r values are better represented by Global NEWS 2, while LM3-FANSY estimates
485 better spatial DON patterns (Tables SI4, SI9, Fig. SI1). Measurement-based estimates are very limited with regard to particulate nutrient compounds. The evaluation of modeled PON is limited to a few measurement-based TKN estimates that include PON, but these aggregate values are matched reasonably well with the model estimates.

https://doi.org/10.5194/gmd-2022-236
Preprint. Discussion started: 2 January 2023

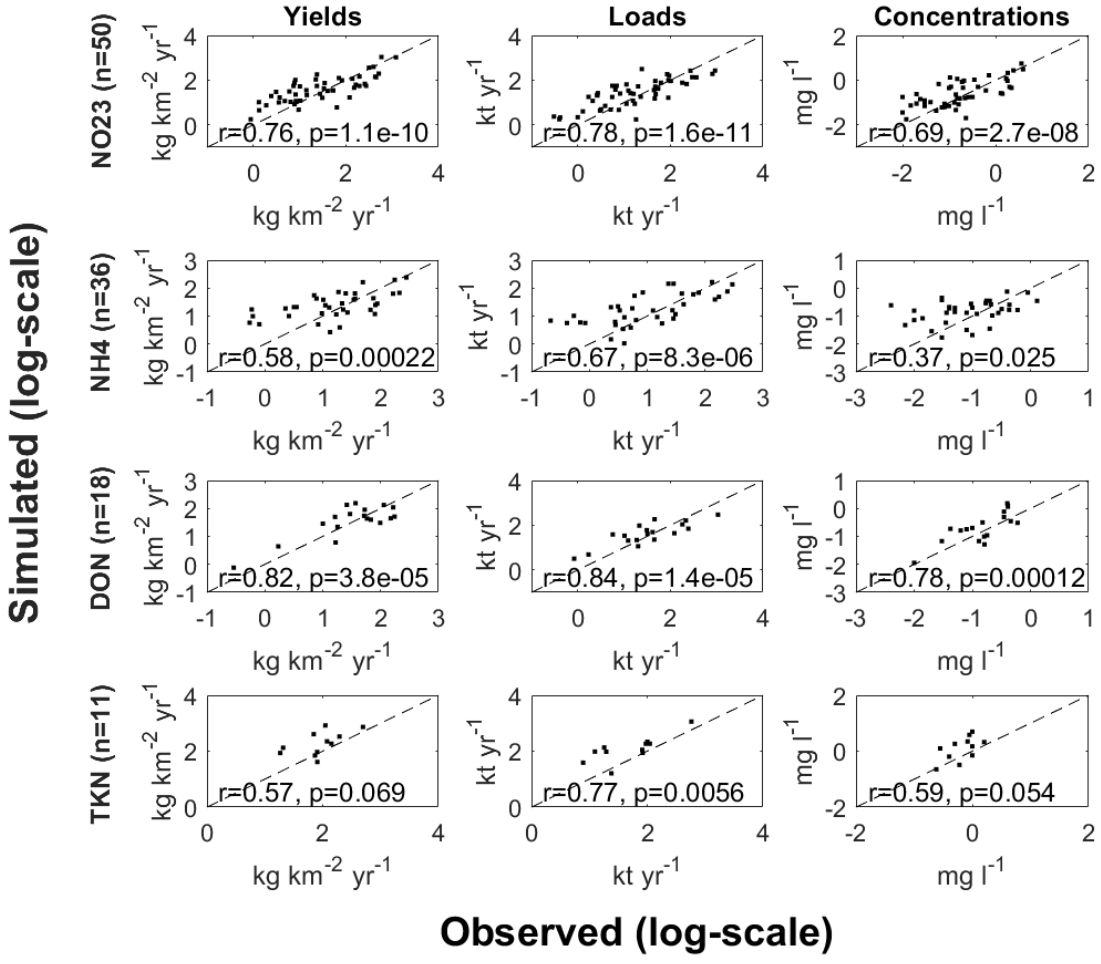

Figure 3: Pearson correlation coefficients (r) and p values (p) between measurement-based vs. simulated NO_{23}, NH_4, DON, and TKN yields, loads, and concentrations across 50, 36, 18, and 11 rivers for the year 1990.

Recent estimates of global river TN loads to the coastal ocean vary widely, ranging from about 36.5 to 47.8 TgN/yr (Table 6, Beusen et al., 2016; Boyer et al., 2006; Galloway et al., 2004; Green et al., 2004; Mayorga et al. 2010). Our global estimate 36.4-41.3 TgN/yr between 1982-2010 is within the published range (Table 5). The distribution among forms for global loads is approximately equally dominated by PON (12.9-15.7 TgN yr^{-1}, 37% of TN), DON (12.0-13.8 TgN yr^{-1}, 34%), and DIN (the sum of NO_{23} and NH_4, 10.6-12.2 TgN yr^{-1}, 30%). The estimates of global river DIN loads are somewhat lower than recent estimates, which range from 14.5 to 18.9 TgN yr^{-1} (Mayorga et al. 2010; Green et al., 2004; Smith et al., 2003). The higher DIN load estimates by previous studies can be partly due to the unconsidered instream removal processes, such as denitrification and algae uptake. In contrast, our global river DON load estimate is slightly higher than a previous estimate 10 TgN yr^{-1} (Harrison et al., 2005). The global river PON load estimate is consistent with a previous estimate, 13.5 TgN yr^{-1} (Mayorga et al. 2010).

https://doi.org/10.5194/gmd-2022-236
Preprint. Discussion started: 2 January 2023

Geoscientific Model Development Discussions

Simulated river PO_4, DOP, and TP yields, loads, and concentrations are in good agreement with the measurement-based estimates across 46, 9, and 5 rivers respectively (Fig. 4, Table 4). Global NEWS 2 has generally higher correlations for yields/loads and lower correlations for concentrations for the three species, compared to LM3-FANSY (Tables SI6-SI8, Fig. SI1). Although only a few estimates of global river TP loads to the coastal ocean exist, our TP estimate of 6.5-7.8 TgP yr^{-1} (Table 5) is within the published range (Table 6), less than a Global NEWS 2 estimate as 9 TgP yr^{-1} (Mayorga e al., 2010) and higher than an IMAGE-GNM estimate as 4 TgP yr^{-1}. LM3-FANSY estimates that globally, rivers export 3.9-4.5 TgP yr^{-1} as PP (58% of TP), 1.9-2.7 TgP yr^{-1} as PO_4 (32%), and 0.6-0.7 TgP yr^{-1} as DOP (10%). The global river PO_4, DOP, and PP load estimates are consistent well with previous estimates of 1.45-2.3 TgP yr^{-1} for PO_4 (Harrison et al., 2010; Smith et al., 2003), 0.6 TgP yr^{-1} for DOP (Harrison et al., 2005), and 6.6 TgP yr^{-1} for PP (Mayorga et al., 2010).

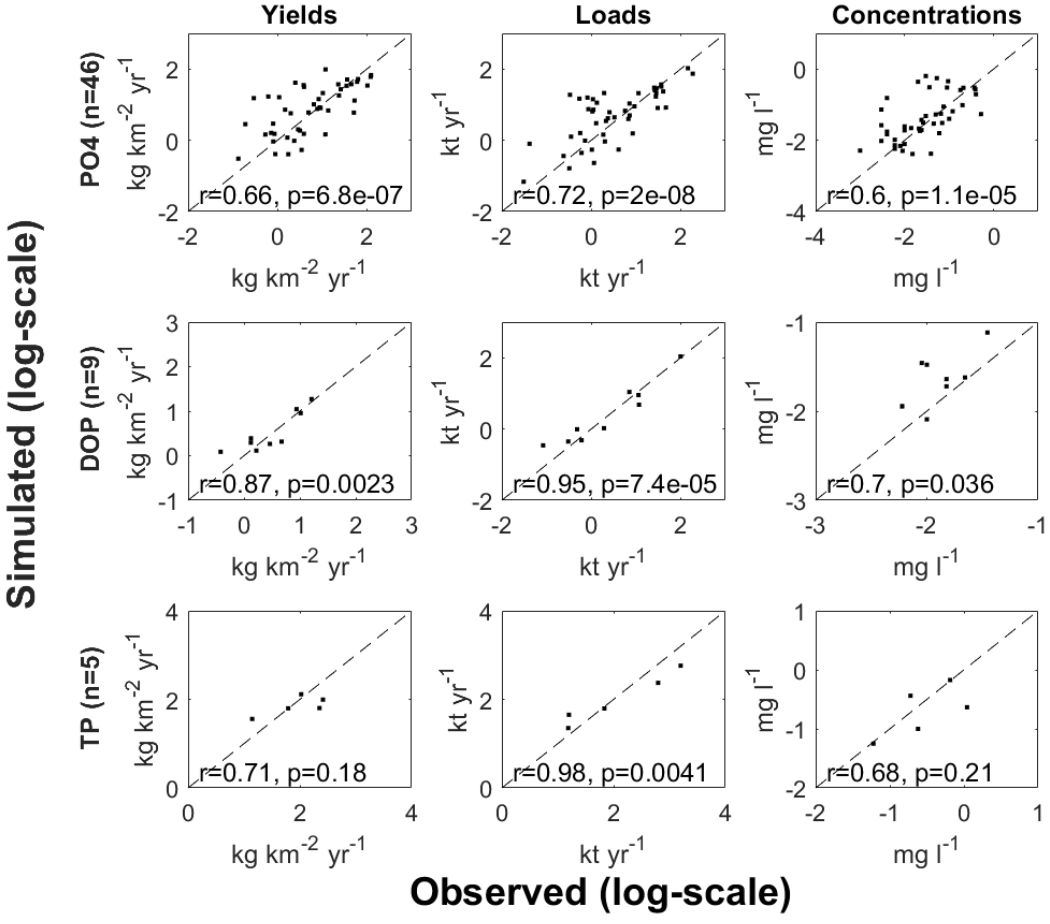

Figure 4: Pearson correlation coefficients (r) and p values (p) between measurement-based vs. simulated PO_4, DOP, and TP yields, loads, and concentrations across 46, 9, and 5 rivers for the year 1990.

https://doi.org/10.5194/gmd-2022-236
Preprint. Discussion started: 2 January 2023

Geoscientific Model Development Discussions

Global watershed model performance of simulating N:P ratios has not been reported in prior publications. Our analysis of model inputs and results indicates that neither LM3-FANSY nor Global NEWS 2 reproduce an observed spatial pattern in DIN:DIP molar ratios across 35 rivers (r = 0.14 for LM3-FANSY, r = 0.11 for Global NEWS 2, Fig. 5, Fig. SI2). Overestimated DIN:DIP molar ratios in 5 artic rivers (i.e., Indigirka, Kolyma, N. Dvian, Yenisey, and Youkon, marked in squares) are largely attributed to underestimated P inputs to these rivers, while the underestimated ratios in the 2 Asian rivers (i.e., Huang He, Zhujiang, marked in circles) are due to both overestimated P inputs and underestimated N inputs. Removing these 7 marked misfits, however, reveals that LM3-FANSY exhibits moderate skill across the 28 remaining rivers (r = 0.61). Thus, while the initial N:P comparison provided herein points to significant challenges to achieving robust N:P simulations across the full range of global systems, it also suggests that notable variations are captured across a subset of systems.

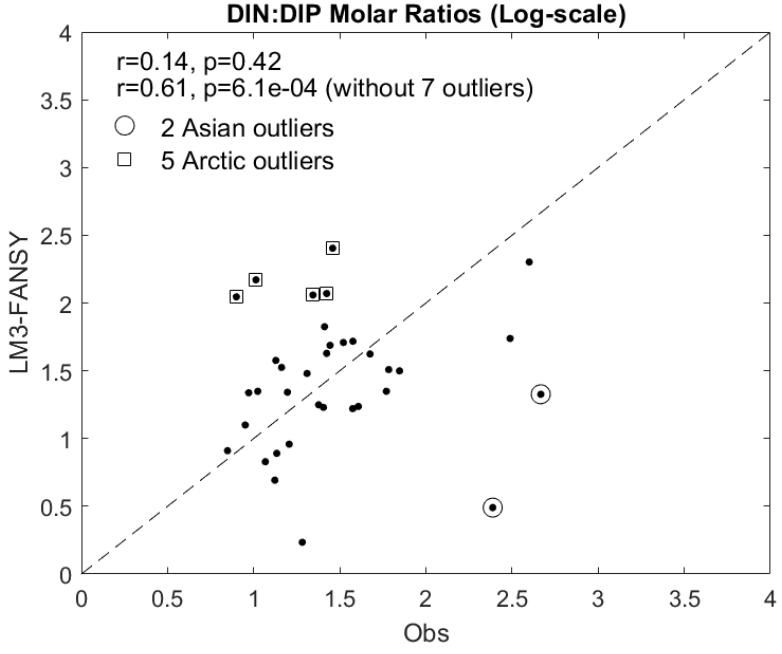

Figure 5: Pearson correlation coefficients (r) and p values (p) between measurement-based vs. simulated river DIN:DIP load molar ratios across 35 rivers for the year 1990.

Despite the significant correlation between the measurement-based and modeled estimates for each solid and nutrient form across various rivers, errors on a basin-by-basin scale are substantial, with high-load, large basins tending to have large absolute errors, as indicated by the log scale. (Figs. 2-4). However, the ranges of prediction errors in our model simulation, as demonstrated in the interquartile range (IQR) and distribution of prediction errors (Table 5), are similar to or smaller than those of other models (Dumont et al., 2005; Harrison et al., 2005; Harrison et al., 2010). These suggest that our model has a

https://doi.org/10.5194/gmd-2022-236
Preprint. Discussion started: 2 January 2023


Geoscientific Model Development Discussions

competitive correlation (r value), precision (IQR), and bias (median error) for each species compared to previous efforts even while including fewer observational constraints on the river sources and more comprehensive and mechanistic freshwater biogeochemical representation.

4.2 Spatial pattern analysis

Spatial maps of river solid and nutrient yields/loads help identify global hotspots of water pollution and provide insight into which processes modulate the magnitudes and form of inputs. A global map of simulated terrestrial soil detachment rate from Eq. (3) is more strongly related to the basin slope map than to the rainfall or LAI maps, reflecting the prominent role of topographic steepness in controlling soil erosion (Fig. 6). This is consistent with previous studies (Pelletier, 2012; Syvitski et al., 2003). The eroded soil is transported as suspended load to rivers, some of which is stored within rivers and lakes, and the rest makes its way to large river outlets to the coastal ocean. Simulated river SS yields are high in mountains like the Andes, Rockies, and Himalayas and low in most gently sloping areas. The yields decrease with distance from mountains, as some of the soil is stored in lowland rivers and lakes and as basin areas (the denominator in yields) increase downstream. In contrast, simulated river SS loads tend to increase downstream, because larger rivers carry more soils from many small streams and tributaries. The Ganges, Changjiang, Indus, and Huang He Rivers in Asia, the Parana and Amazon Rivers in South America, and Mississippi and Columbia in North America are the among the largest river SS exporters (i.e., highest loads) in LM3-FANSY.

The Mississippi, Chang Jiang, Ganges, Ob, Amazon, Parana, Orinoco, and Zaire Rivers are among the top exporters of all three N forms (DIN, DON, and PON) to the coastal ocean in LM3-FANSY (Fig. 7). These basins are characterized by tropical humid climates with high terrestrial productivity, high population/agricultural pressures, or high river water discharge. The highest river DIN yields/loads occurring in European and Asian rivers (e.g., Rine, Elbe, Danube, and Zhujiang), despite their relatively low river water discharge and small basin areas, are largely due to substantial anthropogenic N inputs (Dumont et al., 2005; Mayorga et al, 2010). In contrast, the lowest river DIN yields/loads are estimated for arid regions and most high latitude basins with low population densities and less intensive agriculture. South American, African, and Asian rivers in humid tropical regions (e.g., Amazon, Parana, Orinoco, Zaire, Ganges, Zhujiang, Hong, Chang jiang) are estimated to produce the largest river DON yields/loads, followed by some North American and Russian Rivers (e.g., Mississippi, Yukon, Ob, and Yenisey). The largest river DON yields/loads from tropical regions, despite lower human pressures, indicate a critical role of non-anthropogenic sources (i.e., terrestrial soil and litter runoff from N-enriched natural forests) in exporting the dissolved organic form (Harrison et al., 2005). Low river DON yields/loads tend to occur in relatively dry regions with low anthropogenic pressures.

The Mississippi, Chang Jiang, Ganges, Amazon, and Danube Rivers are among the highest exporters of all three P forms (DIP, DOP, and PP (the sum of POP and PIP)) to the coastal ocean (Fig. 8). Hot spots for river PO_4 yields/loads tend to

https://doi.org/10.5194/gmd-2022-236
Preprint. Discussion started: 2 January 2023

occur in river basins including densely populated large urban centers, such as Chang Jiang, Huang He, Mekong, Shatt el Arab, Ganges, Godavari, Narmada, and Danube. The critical role of urban areas with sewage effluents in producing high river PO_4 yields is consistent with previous studies (Harrison et al., 2010; Mayorga et al., 2010). High river PO_4 yields also occur in humid river basins characterized by high P weathering rates, such as Amazon, Parana, Zaire, Niger, Ganges, Chang jiang, and Mekong or in river basins including intensively farmed areas like Mississippi (Harrison et al., 2010). Highest DOP and PP yields/loads tend to follow a pattern similar to that of PO_4, but there are also differences in patterns of PO_4 yields from patterns of PP yields. The differences, in part, result from deforestation and agricultural expansion in river basins like Columbia and Amur demonstrating elevated PP yields in comparison to PO4 yields (Harrison et al., 2019).

https://doi.org/10.5194/gmd-2022-236
Preprint. Discussion started: 2 January 2023

Geoscientific Model Development Discussions

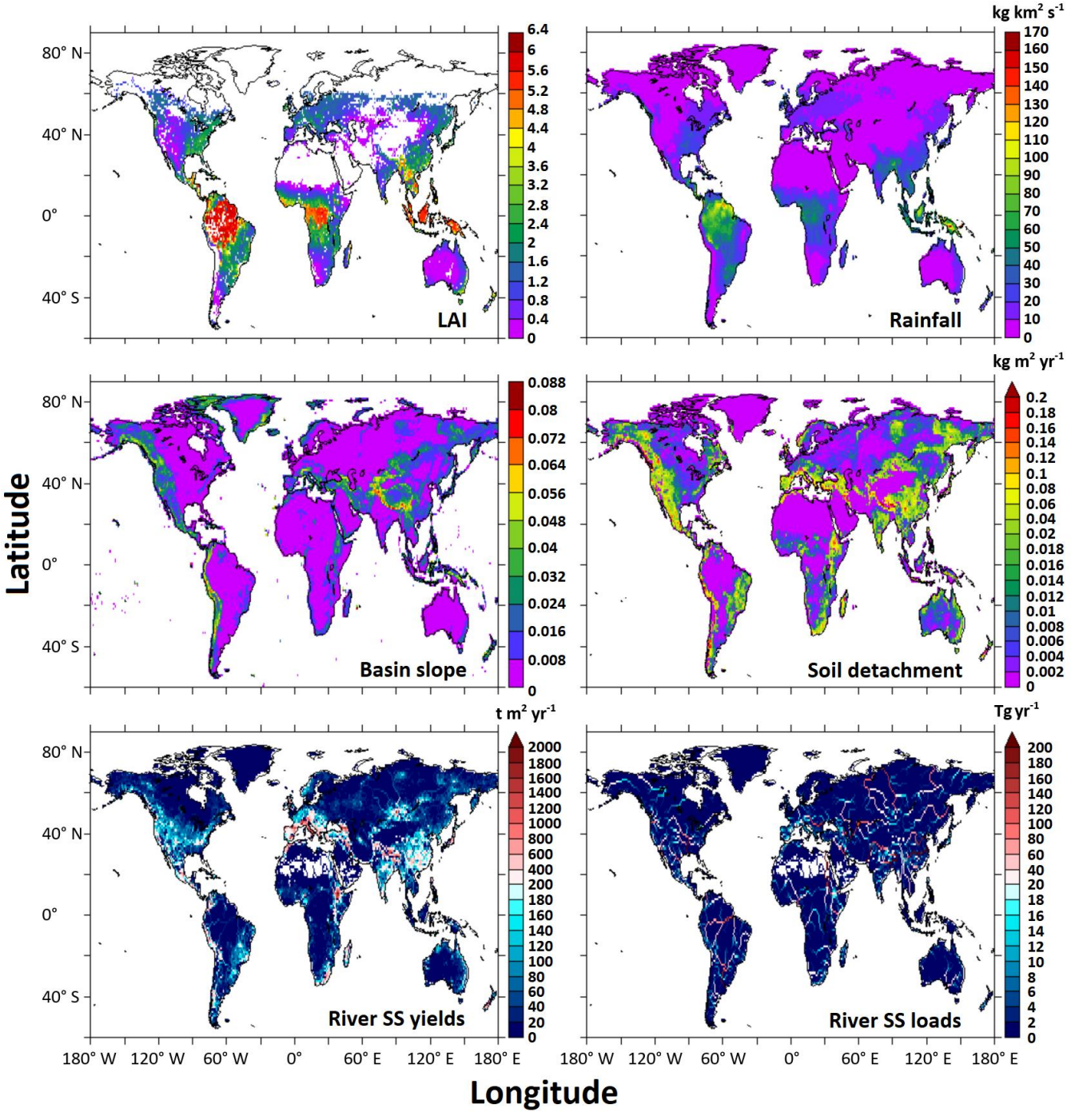

Figure 6: Global maps of model inputs of LAI, rainfall, and basin slope and of simulated soil detachment rate, river SS yields and loads for the year 1990.

https://doi.org/10.5194/gmd-2022-236
Preprint. Discussion started: 2 January 2023

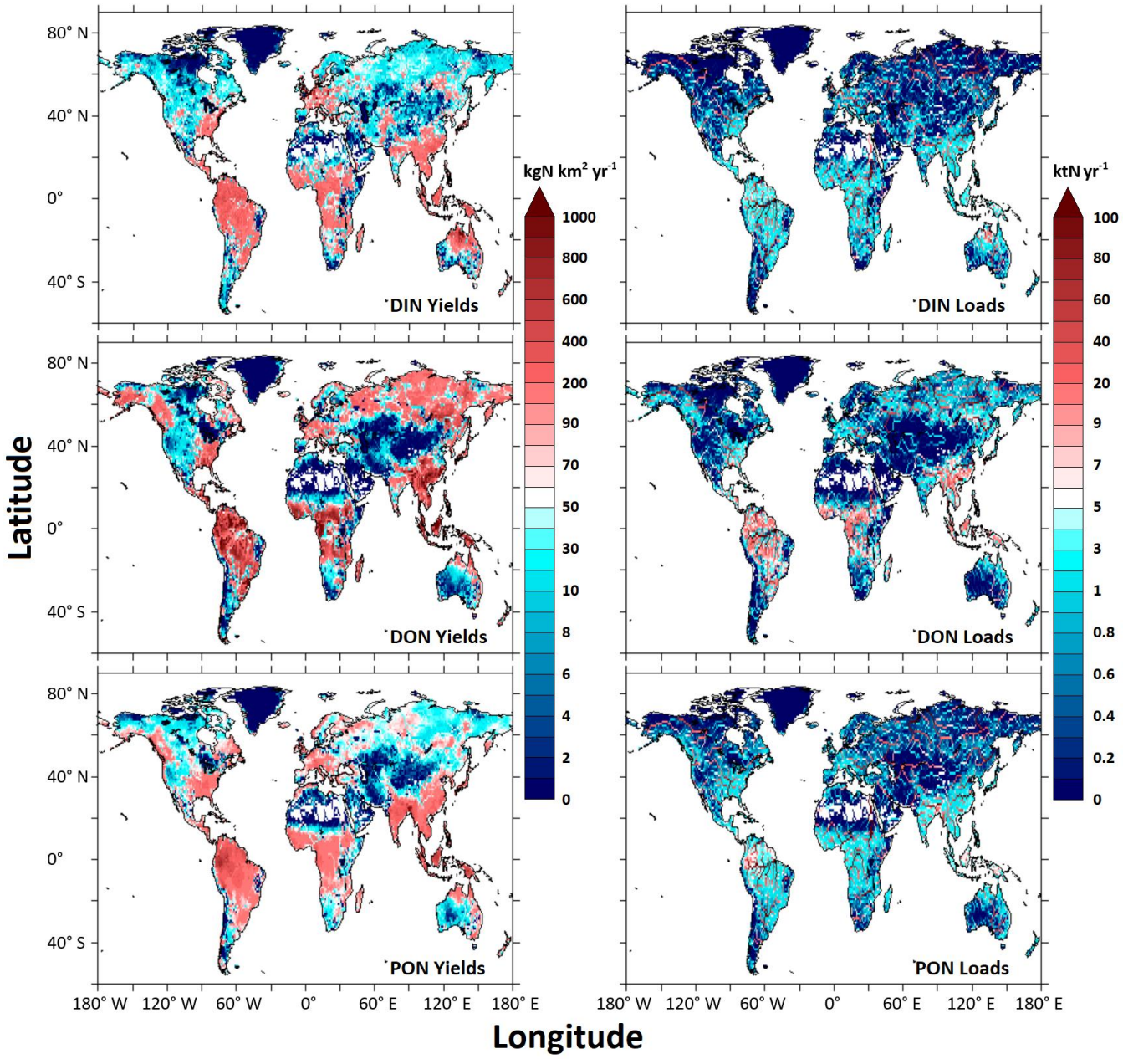

Figure 7: Global maps of simulated river DIN, DON, and PON yields and loads for the year 1990.

https://doi.org/10.5194/gmd-2022-236
Preprint. Discussion started: 2 January 2023

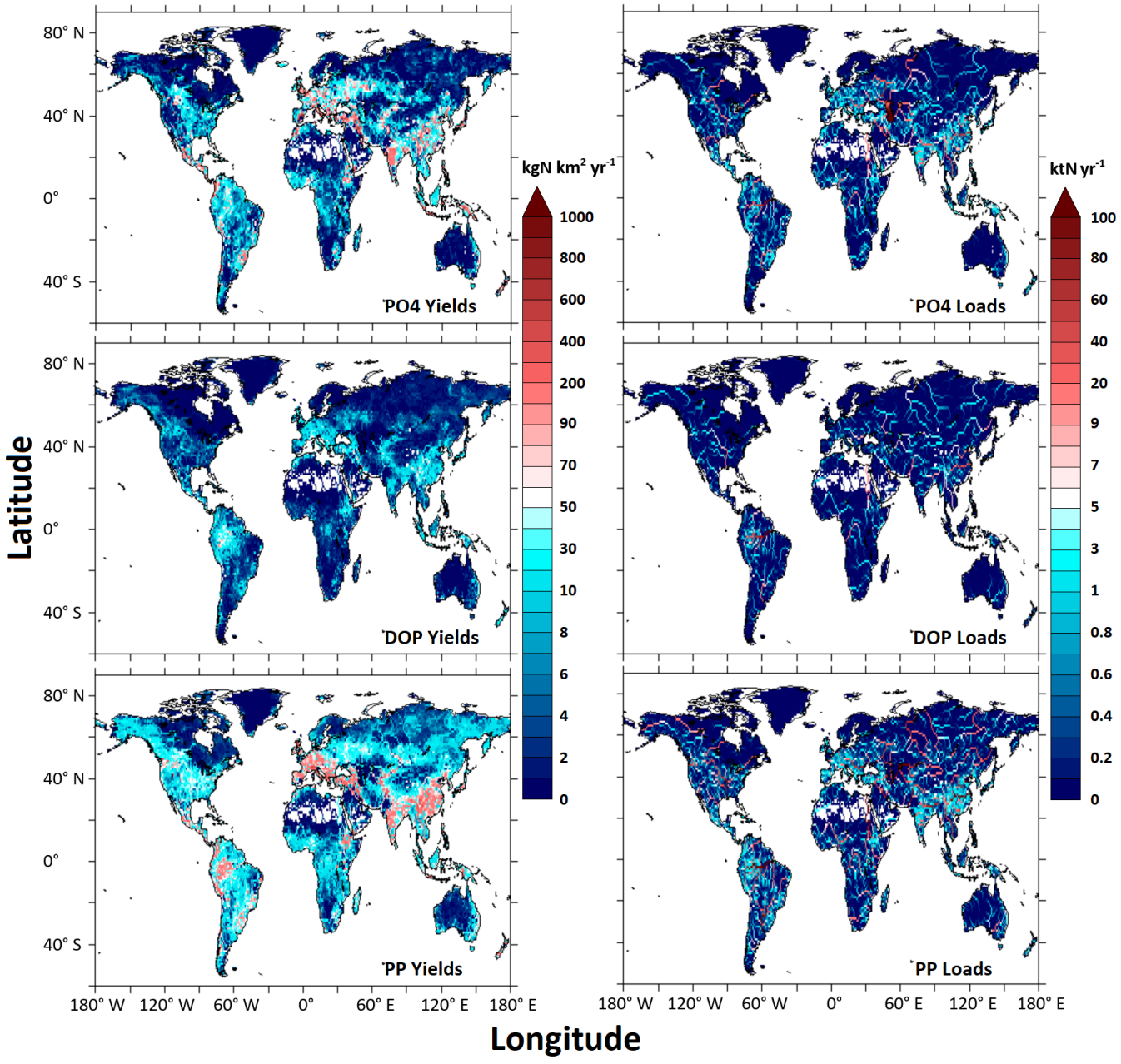

590 **Figure 8: Global maps of simulated river PO_4, DOP, and PP yields and loads for the year 1990.**

4.3 Nutrient composition implications

Simulated high river DIN and DIP yields/loads in Asian, European, and North American regions (Figs. 7 and 8) explain documented severe coastal eutrophication in those regions (e.g. Gulf of Mexico (Turner et al., 2008), Baltic Sea (Eriksson et

https://doi.org/10.5194/gmd-2022-236
Preprint. Discussion started: 2 January 2023

595 al., 2007, Conley, 2012), Wadden Sea (Van Beusekom, 2018), North Sea (Van Beusekom ,2018), and Yellow Sea (Liu et al., 2013)). This severe coastal eutrophication largely results from dissolved inorganic nutrients (e.g., DIN and DIP) being readily bioavailable forms to play disproportionately important roles in aquatic ecosystem function (e.g., primary production) compared to less labile organic forms (Sipler and Bronk, 2004). Relatively few eutrophication problems reported in South American and African regions with high DIN and DIP yields/loads may be, in part, due to limited samplings and 600 observations in these regions.

Reported proliferation of some harmful phytoplankton species also appears to coincide with regions where DIN and DIP yields are high and anthropogenic sources dominate those yields (Glibert et al., 2008). It is generally accepted that nonpoint, fertilizer applications are the dominant sources of river DIN loads, while point, sewage sources play a prominent role in 605 determining river DIP loads (Smith et al., 2003; Harrison et al., 2010). The delivery of terrestrial DIN and DIP to surface waters are expected to further increase with population growth, agricultural expansion and intensification, and construction of sewers in developing countries (Alcamo et al., 2005). These together highlight that agricultural yield increasing technologies (e.g., breeding, biotechnology traits), advances in agronomic practices (e.g., 4Rs: applying the right source of nutrients, at the right rate, at the right time, in the right place), efficient livestock nutrition and waste management (e.g., 610 shifts towards mixed crop-livestock systems), and adoption of sustainable, low-meat diets with low food waste (Cui et al., 2018; Dietrich et al., 2014; Edgerton et al., 2009; Johnston and Bruulsema, 2014; Popp et al., 2017; Weindl, et al., 2015) are critical in preventing further deterioration of DIN and DIP associated problems.

Although the likelihood for a harmful algal species to bloom depends on complex factors (Anderson et al., 2021), the global 615 distribution of TN:TP ratios has an implication for outbreaks of some HABs. Regions with TN:TP molar ratios of river loads falling below Redfield proportions in our simulation (blue circles, Fig. 9) coincide with regions where below-Redfield or below-normal TN:TP ratios have been related to increased abundance of certain harmful species (e.g., Tolo Harbor in Hong Kong (Hodgkiss, 2001), Tunisian aquaculture lagoons (Romdhane et al., 1998), Dutch coastal waters (Riegman, 1995), and western Florida shelf (Heil et al., 2007)). Although increasing N:P ratios in fertilizers since the 1970s (FAO, 2015) explain 620 overall higher TN:TP ratios of inputs to rivers than those of river loads to the coastal ocean (Fig. 9), decreasing TN:TP ratios from the land to ocean continuum indicates that much of N has been removed via freshwater denitrification, while P has been retained within the freshwater systems more efficiently than N during the transformations and transport. Continuously increasing fertilizer N:P ratios may cause more prevalent P limitation, resulting in P additions to ecosystems with even greater impacts than under present conditions. Freshwater systems, however, may play a critical role in modulating the 625 altered terrestrial TN:TP ratios before reaching the coastal ocean.

https://doi.org/10.5194/gmd-2022-236
Preprint. Discussion started: 2 January 2023

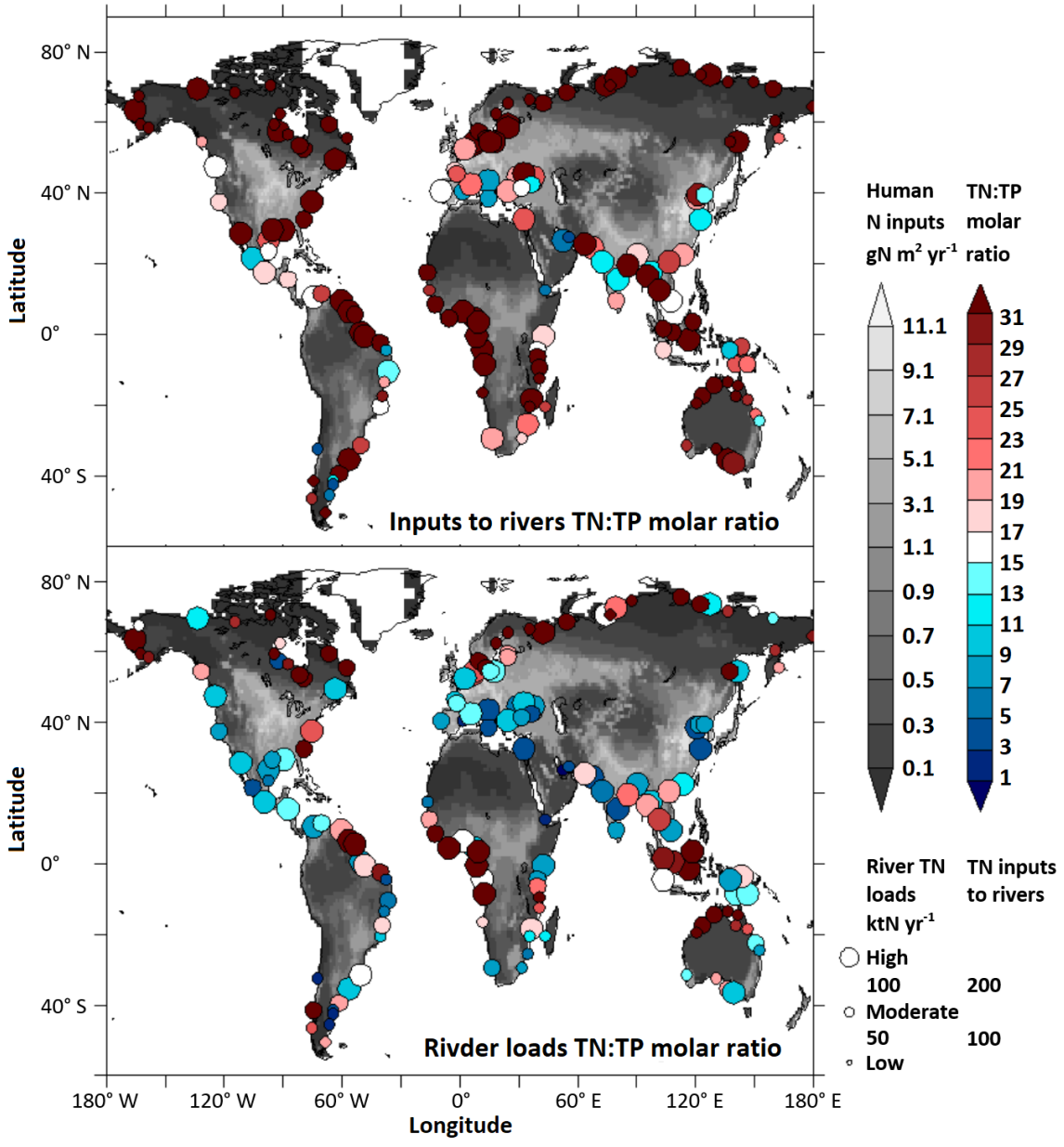

Figure 9: Maps of simulated TN:TP molar ratios of nutrients inputs to rivers vs. rivers loads to the coastal ocean.

4.4 Model sensitivity with changes in parameter settings and nutrient inputs

The one free parameter of terrestrial soil detachment component (C_1) plays a significant role in determining the overall amount of river SS loads, with ±15% changes in the parameter leading to ±13% changes in global river SS loads (Table 5).

https://doi.org/10.5194/gmd-2022-236
Preprint. Discussion started: 2 January 2023


Geoscientific Model Development Discussions

Increases (decreases) in SS loads also modestly enhance (reduce) sorption of PO_4 to solid particles, as indicated by PO_4 and PP changes (Table 5). The parameter is, however, less vital in explaining spatial distribution of river SS, PO_4, and PP loads (Table 4).

A sensitivity analysis, in which each nutrient input source was increased by 15%, suggests that the model results are fairly robust to these input increases, which do not enhance the skill of spatial river nutrient patterns reflected in r values (Table 4) and increase nutrient loads by ~15% for cases of terrestrial soil and litter runoffs, and in most cases, substantially less (~5%, Table 5). Removing each nutrient input source and examining the response in model outputs suggests that terrestrial soil runoff is the most dominant source of river N loads, followed by terrestrial litter runoff and wastewater (Table 5). For river P loads, terrestrial soil runoff is also the most dominant source, but unlike for N, the second largest source is weathering, followed by terrestrial litter runoff and wastewater. Terrestrial soil and litter runoff, and weathering are also important sources in explaining spatial distribution of river nutrients in inorganic and dissolved organic forms (Table 4). Removals of these sources reduce r values for NO_{23}, NH_4, PO_4, DON, and DOP, compared to those driven by the other source removals. Removal of aquaculture and atmospheric deposition have less impacts on both r values and quantities, suggesting that inaccuracies in these inputs have minor impacts on regional and global model estimates, relative to the inaccuracies associated with the other model inputs. However, the importance of each source is likely to vary, depending on the dominant control on river nutrient loads in a specific region.

An analysis of the model sensitivity simulation, wherein the dynamic contributors to light extinction (i.e., ISS, POM, and CHL from Eq. (22)) were removed, suggests that proper light limitation of phytoplankton growth is particularly important for skillful estimates of river inorganic and organic nutrient loads. Removing the dynamic light shading component leads to a ~6%, ~45%, and ~93% overestimation of 1982-2010 mean river organic nutrient (DON, PON, and DOP) loads, while it drives underestimated river inorganic nutrient (DIN and DIP) loads by ~9% and ~40% respectively (Table 5). Inorganic nutrient levels are suppressed by invigorated phytoplankton populations without the light attenuation impacts of ISS, POM and CHL and more nutrients end up in organic forms. Phytoplankton controls thus offer an effective means of calibrating the mix of inorganic and organic constituents. The absence of the component also reduces r values modestly (Table 4). The model predictions of river solids and nutrients in spatial distribution and magnitude are relatively insensitive to ±15% changes in the PO4 sorption/resorption parameters (a and b) from Eq. (40). The denitrification rate coefficient of ±15% changes leads to -5% and 11% changes in global river DIN loads (Table 5), yet the coefficient has less impacts on spatial distribution of river nutrient and solid loads (Table 4).

https://doi.org/10.5194/gmd-2022-236
Preprint. Discussion started: 2 January 2023


Geoscientific Model Development Discussions

5 Conclusion

Our comparisons of process-based LM3-FANSY outputs with measurement-based estimates across world major rivers demonstrate skillful simulations for most riverine constituents despite being restricted to a universal parameter set – the same parameters for all the basins (i.e., without tuning of each basin). Although LM3-FANSY is capable of producing river solids and nutrients in various forms and units (SS, NO_{23}, NH_4, DIN, DON, PON, PO_4, DOP, PIP, POP, and PP yields, loads, and concentrations), some disagreement between the modeled and measurement-based estimates remain. Many observational studies have noted the uncertainties associated with measurement methods, location, and frequency that likely contribute to these disagreements. There is also significant room for further model improvement. As the land model LM3 is improved and extended to include terrestrial P dynamics, there will be opportunities to greatly improve estimates of soil P storage and runoff to streams and rivers. The sensitivity and DIN:DIP molar ratio analyses also suggest that simulations of river nutrient loads may be improved markedly through improvements to global datasets including runoff, wastewater, and weathering. In addition, anthropogenic hydraulic controls are expected to increase in the future (Seitzinger et al., 2010). It will be thus important to consider the effects of such controls, such as large dams that can impound solids and nutrients to substantially decrease their loadings to rivers (Vorosmarty et al., 2003). Finally, all of these model improvement efforts will be greatly facilitated by extensive river measurements across the world, with a better assessment of uncertainties.

LM3-FANSY represents a significant step forward in terms of capacity to model coupled algae, SS, N, and P dynamics in freshwaters at a process-based, spatially explicit, global scale. Although this study is focused on model development and descriptions, the capability of LM3 to simulate changes in vegetation and soil nutrient storage in response to the aforementioned, many terrestrial dynamics under subannual to centurial historical climate and land use changes (Lee et al., 2016; Lee et al., 2019; Lee et al., 2021) allows applications of LM3-FANSY for studies of temporal (subannual to multiyear) variability and long-term trends in global and regional water pollution. Therefore, LM3-FANSY can serve as a baseline for studies aimed at understanding the effects of terrestrial perturbations on coastal eutrophication. The mechanistic modeling framework of LM3-FANSY is also well suited to make future projections by use of a new generation of future socioeconomic and climate scenarios over centuries.

Code availability

The LM3-FANSY v1.0 code was written in Fortran. The complete code has been archived on Zenodo (https://doi.org/10.5281/zenodo.7457981, Lee, 2022) and is available on GitHub (https://github.com/minjinl/LM3-FANSY, last access: 21 December 2022).

https://doi.org/10.5194/gmd-2022-236
Preprint. Discussion started: 2 January 2023


Geoscientific Model Development Discussions

Data availability

All reported data, model inputs and outputs used to produce figures are available in the Supplement.

Author contribution

M. Lee and C. A. Stock developed the FANSY model and wrote major portions of the manuscript with substantial inputs from J. P. Dunne and E. Shevliakova. M. Lee performed the model simulations and analyses. All authors analyzed and discussed the results.

Competing interests

The authors declare that they have no conflict of interest.

Acknowledgments

Award NA18OAR4320123 from the National Oceanic and Atmospheric administration, U.S. Department of Commerce (ML). The statements, findings, conclusions, and recommendations are those of the authors and do not necessarily reflect the views of the National Oceanic and Atmospheric Administration, or the U.S. Department of Commerce. We thank Fabien Paulot from NOAA/GFDL and Cristina Schultz from Princeton University for their incisive comments on the manuscript. We thank Nathaniel Chaney from Duke University for providing us the slope data.

References

Alcamo J, van Vuuren D, Cramer W, Alder J, Bennett EM, Carpenter SR, Christiensen J, Foley JA, Maerker M, Masui T et al.: Changes in ecosystem services and their drivers across the scenarios. Ecosyst Hum Well-Being 2005, 2:297-373.

Anderson, D. M., Fensin, E., Gobler, C. J., Hoeglund, A. E., Hubbard, K. A., Kulis, D. M., Landsberg, J. H., Lefebvre, K. A., Provoost, P., Richlen, M. L., Smith, J. L., Solow, A. R., and Trainer, V, L.: Marine harmful algal blooms (HABs) in the United States: History, current status and future trends, Harmful Algae, 102, 1568-9883, 2021.

Anderson, D. M., Glibert, P. M., and Burkholder, J. M.: Harmful algal blooms and eutrophication: Nutrient sources, composition, and consequences, Estuaries, 25, 704–726, 2002.

Beusen, A. H. W., Bouwman, A. F., Van Beek, L. P. H., Mogollón, J. M., and Middelburg, J. J.: Global riverine N and P transport to ocean increased during the 20th century despite increased retention along the aquatic continuum, Biogeosciences, 13, 2441–2451, 2016.

https://doi.org/10.5194/gmd-2022-236
Preprint. Discussion started: 2 January 2023

Beusen, A. H. W., Dekkers, A. L. M., Bouwman, A. F., Ludwig, W., and Harrison, J.: Estimation of global river transport of sediments and associated particulate C, N, and P, Global Biogeochem. Cy., 19, GB4S05, 2005.

Beusen, A. H. W., Van Beek, L. P. H., Bouwman, A. F., Mogollón, J. M., and Middelburg, J. J.: Coupling global models for hydrology and nutrient loading to simulate nitrogen and phosphorus retention in surface water – description of IMAGE–GNM and analysis of performance, Geosci. Model Dev., 8, 4045–4067, 2015.

Billen, G., Garnier, J., and Hanset, P.: Modelling phytoplankton development in whole drainage networks: The riverstrahler model applied to the Seine River system, Hydrobiologia, 289, 119–137, 1994.

Bowie, G. L., Mills, W. B., Porcella, D. B., Campbell, C. L., Pagenkopf, J. R., Rupp, G. L., Johnson, K. M., Chan, P. W. H., and Gherini, S. A.: Rates, constants, and kinetics formulations in surface water quality modeling, Athens, Georgia, 1985.

Boyer, E. W., Howarth, R. W., Galloway, J. N., Dentener, F. J., Green, P. A., and Vorosmarty, C. J.: Riverine nitrogen export from the continents to the coasts, Global Biogeochem. Cy., 20, GB1S91, 2006.

Chapra, S. C.: Surface Water-Quality Modeling, Waveland Press, Long Grove, IL, USA, 1997.

CMIP6 Forcing Datasets Summary: https://docs.google.com/document/d/1pU9IiJvPJwRvIgVaSDdJ4O0Jeorv_2ekEtted34K9cA/edit/, last access: 9 April 2022.

Conley, D. J.: Save the Baltic Sea, Nature, 486, 463–464, 2012.

Cordell, D., Drangert, J., and White, S.: The story of phosphorus: Global food security and food for thought, Glob. Environ. Change, 19, 292-305, 2009.

Cui, Z., Zhang, H., Chen, X., Zhang, C., Ma, W. et al.: Pursuing sustainable productivity with millions of smallholder farmers, Nature, 555, 363–366, 2018.

Danielson, J. J. and Gesch, D. B.: Global multi-resolution terrain elevation data 2010 (GMTED2010): U.S. Geological Survey Open-File Report 2011–1073, https://pubs.usgs.gov/of/2011/1073/pdf/of2011-1073.pdf, 2011.

Diaz, R. J. and Rosenberg, R.: Spreading dead zones and consequences for marine ecosystems, Science, 321, 926–929, 2008.

Dietrich, J. P., Schmitz, C., Lotze-Campen, H., Popp, A., and Müller, C.: Forecasting technological change in agriculture—An endogenous implementation in a global land use model, Technol. Forecast Soc. Change, 81, 236-249, 2014.

Dio Toro, D. M.: Optics of turbid estuarine waters: approximations and applications, Water Res., 12, 1059–1068, 1976.

Dumont, E., Harrison, J. A., Kroeze, C., Bakker, E. J., and Seitzinger, S. P.: Global distribution and sources of dissolved inorganic nitrogen export to the coastal zone: Results from a spatially explicit, global model, Global Biogeochem. Cy., 19, GB4S02, 2005.

Dunne, J. P., Armstrong, R. A., Gnanadesikan, A., and Sarmiento, J. L.: Empirical and mechanistic models for the particle export ratio, Global Biogeochem. Cy., 19, GB4026, 2005.

Edgerton, M. D.: Increasing Crop Productivity to Meet Global Needs for Feed, Food, and Fuel, Plant Physiol., 149, 7–13, 2009.

Eppley, R. W.: Temperature and phytoplankton growth in the sea, Fish. Bull., 70, 1063–1085, 1972.

https://doi.org/10.5194/gmd-2022-236
Preprint. Discussion started: 2 January 2023

Eriksson H, Pastuszak M, Lofgren S, Morth C and Humborg C.: Nitrogen budgets of the Polish agriculture 1960–2000: implications for riverine nitrogen loads to the Baltic Sea from transitional countries, Biogeochemistry, 85, 153–68, 2007.

FAO (Food and Agriculture Organization of the United Nations): FAOSTAT database, Fertilizers by Nutrient, https://www.fao.org/faostat/en/#data/RFN, 2022.

Ferguson, R. I., and Church, M.: A simple universal equation for grain settling velocity, J. Sediment. Res., 74, 933–937, 2004.

Fowler, D., Coyle, M., Skiba, U., Sutton, M. A., Cape, J. N., Reis, S., Sheppard, L. J., Jenkins, A., Grizzetti, B., Galloway, J. N., Vitousek, P., Leach, A., Bouwman, A. F., Butterbach-Bahl, K., Dentener, F., Stevenson, D., Amann, M., and Voss, M.: The global nitrogen cycle in the twenty-first century, Phil. Trans. R. Soc. B, 368: 20130164, 2013.

Frost, B. W. and Franzen, N. C.: Grazing and iron limitation in the control of phytoplankton stock and nutrient concentration: a chemostat analogue of the Pacific equatorial upwelling zone, Mar. Ecol. Prog. Ser., 83, 291–303, 1992.

Galloway, J. N., Dentener, F. J., Capone, D. G., Boyer, E. W., Howarth, R. W., Seitzinger, S. P., Asner, G. P., Cleveland, C. C., Green, P. A., Holland, E. A., Karl, D. M., Michaels, A. F., Porter, J. H., Townsend, A. R., and Vöosmarty, C. J.: Nitrogen cycles: past, present, and future, Biogeochemistry, 70, 153–226, 2004.

Garnier, J., Nemery, J., Billen, G., and Thery, S.: Nutrient dynamics and control of eutrophication in the Marne River system: modelling the role of exchangeable phosphorus, J. Hydrol., 304, 397–412, 2005.

Geider, R. J., MacIntyre, H. L., and Kana, T. M.: Dynamic model of phytoplankton growth and acclimation: responses of the balanced growth rate and the chlorophyll a:carbon ratio to light, nutrient-limitation and temperature, Mar. Ecol. Prog. Ser., 148, 187-200, 1997.

Gerber, S., Hedin, L. O., Oppenheimer, M., Pacala, S. W., and Shevliakova, E.: Nitrogen cycling and feedbacks in a global dynamic land model, Glob. Biogeochem. Cy., 24, GB1001, 2010.

Glibert, P. M., Magnien, R., Lomas, M. W., Alexander, J., Fan, C., Haramoto, E., Trice, M., and Kana, T. M.: Harmful algal blooms in the Chesapeake and Coastal Bays of Maryland, USA: Comparison of 1997, 1998, and 1999 events, Estuaries, 24, 875–883, 2001.

Glibert, P. M., Mayorga, E., and Seitzinger, S.: Prorocentrum minimum tracks anthropogenic nitrogen and phosphorus inputs on a global basis: Application of spatially explicit nutrient export models, Harmful Algae, 8, 33-38, 2008.

Glibert, P. M. and Terlizzi, D. E.: Cooccurrence of elevated urea levels and dinoflagellate blooms in temperate estuarine aquaculture ponds, Appl. Environ. Microbiol., 65, 5594–5596, 1999.

Green, P. A., Vörösmarty, C. J., Meybeck, M., Galloway, J. N., Peterson, B. J., and Boyer, E. W.: Pre-industrial and contemporary fluxes of nitrogen through rivers: a global assessment based on typology, Biogeochemistry, 68, 71–105, 2004.

Harrison, J. A., Beusen, A. H. W., Fink, G., Tang, T., Strokal, M., Bouwman, A. F., Metson, G. S., and Vilmin, L.: Modeling phosphorus in rivers at the global scale: recent successes, remaining challenges, and near-term opportunities, Curr. Opin. Environ. Sustain., 36, 68-77, 2019.

https://doi.org/10.5194/gmd-2022-236
Preprint. Discussion started: 2 January 2023

Harrison, J. A., Bouwman, A. F., Mayorga, E., and Seitzinger, S.: Magnitudes and sources of dissolved inorganic phosphorus inputs to surface fresh waters and the coastal zone: A new global model, Global Biogeochem. Cy., 24, GB1003, 2010.

Harrison, J. A., Caraco, N., and Seitzinger, S. P.: Global patterns and sources of dissolved organic matter export to the coastal zone: Results from a spatially explicit, global model, Global Biogeochem. Cy., 19, GB4S04, 2005.

Hatono, M. and Yoshimura, K.: Development of a global sediment dynamics model, Prog. Earth Planet. Sci., 7, 59, 2020.

Heil, C. A., Revilla, M., Glibert, P. M., and Murasko, S.: Nutrient quality drives phytoplankton community composition on the West Florida Shelf, Limnol. Oceanogr., 52, 1067–1078, 2007.

Heisler, J., Glibert, P. M., Burkholder, J. M., Anderson, D. M., Cochlan, W., Dennison, W. C., Dortch, Q., Gobler, C. J., Heil, C. A., Humphries, E., Lewitus, A., Magnien, R., Marshallm, H. G., Sellner, K., Stockwell, D. A., Stoecker, D. K., and Suddleson, M.: Eutrophication and harmful algal blooms: A scientific consensus, Harmful Algae, 8, 3–13, 2008.

Hodgkiss, I. J.: The N:P ratio revisited, in: Prevention and Management of Harmfifl Algal Blooms in the South China Sea, edited by: Ho, K. C. and Wang, Z. D., School of Science and Technology, The Open University of Hong Kong, China, 2001.

Howarth, R. W. and Marino, R.: Nitrogen as the limiting nutrient for eutrophication in coastal marine ecosystems: Evolving views over three decades, Limnol. Oceanogr., 51, 364–376, 2006.

Hurtt, G. C., Chini, L., Sahajpal, R., Frolking, S., Bodirsky, B. L., Calvin, K., Doelman, J. C., Fisk, J., Fujimori, S., Klein Goldewijk, K., Hasegawa, T., Havlik, P., Heinimann, A., Humpenöder, F., Jungclaus, J., Kaplan, J. O., Kennedy, J., Krisztin, T., Lawrence, D., Lawrence, P., Ma, L., Mertz, O., Pongratz, J., Popp, A., Poulter, B., Riahi, K., Shevliakova, E., Stehfest, E., Thornton, P., Tubiello, F. N., van Vuuren, D. P., and Zhang, X.: Harmonization of global land use change and management for the period 850–2100 (LUH2) for CMIP6, Geosci. Model Dev., 13, 5425–5464, 2020.

Johnston, A. M. and Bruulsema, T. W.: 4R Nutrient Stewardship for Improved Nutrient Use Efficiency, Procedia Eng., 83, 365–370, 2014.

Kaushal, S., Groffman, P. M., Band, L. E., Shields, C. A., Morgan, R. P., Palmer, M. A., Belt, K. T., Swan, C. M., Findlay, S. E. G., and Fisher, G. T.: Interaction between urbanization and climate variability amplifies watershed nitrate export in Maryland, Environ. Sci. Technol., 42, 5872–8, 2008.

Kemp, W. M., Boynton, W. R., Adolf, J. E., Boesch, D. F., Boicourt, W. C., Brush, G., Cornwell, J. C., Fisher, T. R., Glibert, P.M., Hagy, J. D., Harding, L. W., Houde, E. D., Kimmel, D. G., Miller, W. D., Newell, R. I. E., Roman, M. R., Smith, E. M., and Stevenson, J.C.: Eutrophication of Chesapeake Bay: historical trends and ecological interactions, Mar. Ecol. Prog. Ser., 303, 1–29, 2005.

Lacoul, P. and Freedman, B.: Environmental influences on aquatic plants in freshwater ecosystems, Environ. Rev., 14, 89-136, 2006.

Lee, M.: minjinl/LM3-FANSY: LM3-FANSY v1.0 (v1.0), Zenodo [code], https://doi.org/10.5281/zenodo.7457981, 2022.

https://doi.org/10.5194/gmd-2022-236
Preprint. Discussion started: 2 January 2023

Lee, M., Malyshev, S., Shevliakova, E., Milly, P. C. D., and Jaffé, P. R.: Capturing interactions between nitrogen and hydrological cycles under historical climate and land use, Susquehanna Watershed analysis with the GFDL Land Model LM3-TAN, Biogeosciences, 11, 5809–5826, 2014.

Lee, M., Shevliakova, E., Malyshev, S., Milly, P. C. D., and Jaffé, P. R.: Climate variability and extremes, interacting with nitrogen storage, amplify eutrophication risk, Geophys. Res. Lett., 43, 7520–8, 2016.

Lee, M., Shevliakova, E., Stock, C. A., Malyshev, S., and Milly, P. C. D.: Prominence of the tropics in the recent rise of global nitrogen pollution, Nat. Commun., 10, 1437, 2019.

Lee, M., Stock, C. A., Shevliakova, E., Malyshev, S., and Milly, P. C. D.: Globally prevalent land nitrogen memory amplifies water pollution following drought years, Environ. Res. Lett., 16, 014049, 2021.

Leong, S. C. Y., Murata, A., Nagashima, Y., and Taguchi, S.: Variability in toxicity of the dinoflagellate Alexandrium tamarense in response to different nitrogen sources and concentrations, Toxicon, 43, 407−415, 2004.

Liu, D., Keesing, J. K., He, P., Wang, Z., Shi, Y., and Wang, Y.: The world's largest macroalgal bloom in the Yellow Sea, China: formation and implications, Estuar. Coast. Shelf Sci., 129, 2–10, 2013.

Liu, X., Stock, C. A., Dunne, J. P., Lee, M., Shevliakova, E., Malyshev, S., and Milly, P. C. D.: Simulated global coastal ecosystem responses to a half-century increase in river nitrogen loads, Geophys. Res. Lett., 48, e2021GL094367, 2021.

Mayorga, E., Seitzinger, S. P., Harrison, J. A., Dumont, E., Beusen, A. H. W., Bouwman, A. F. Fekete, B. M., Kroeze, C., Van Drecht, G.: Global Nutrient Export from WaterSheds 2 (NEWS 2): Model development and implementation, Environ. Model. Softw., 25, 837-853, 2010.

McGechan, M. B. and Lewis, D. R.: Sorption of phosphorus by soil, part 1: principles, equations and models, Biosyst. Eng., 82, 1–24, 2002.

McLaughlin, C. J., Smith, C. A., Buddemeier, R. W., Bartley, J. D., and Maxwell, B. A.: Rivers, runoff, and reefs, Glob. Planet. Change, 39, 191-199, 2003.

Meinshausen, M., Vogel, E., Nauels, A., Lorbacher, K., Meinshausen, N., Etheridge, D. M., Fraser, P. J., Montzka, S. A., Rayner, P. J., Trudinger, C. M., Krummel, P. B., Beyerle, U., Canadell, J. G., Daniel, J. S., Enting, I. G., Law, R. M., Lunder, C. R., O'Doherty, S., Prinn, R. G., Reimann, S., Rubino, M., Velders, G. J. M., Vollmer, M. K., Wang, R. H. J., and Weiss, R.: Historical greenhouse gas concentrations for climate modelling (CMIP6), Geosci. Model Dev., 10, 2057–2116, 2017.

Meybeck, M. and Ragu, A.: GEMS-GLORI world river discharge database, https://doi.org/10.1594/PANGAEA.804574, 2012.

Milly, P. C. D., Malyshev, S., Shevliakova, E., Dunne, K. A., Findell, K. L., Gleeson, T., Liang, Z., Phillipps, P., Stouffer, R. J., and Swenson, S.: An enhanced model of land water and energy for global hydrologic and earth-system studies, J. Hydrometeorol., 15, 1739–1761, 2014.

Nemery, J.: Origine et devenir du phosphore dans le continuum aquatique de la Seine, des petits basins a` l'estuaire. Roˆle du phosphore e´changeable sur l'eutrophisation, Ph.D. thesis, University of Paris, France, 258 pp., 2003.

https://doi.org/10.5194/gmd-2022-236
Preprint. Discussion started: 2 January 2023

Paerl, H. W., Otten, T. G., and Kudela, R.: Mitigating the expansion of harmful algal blooms across the freshwater-to-marine continuum, Environ. Sci. Technol., 52, 5519–5529, 2018.

Parsons, M. L., Dortch, Q., and Turner, R. E.: Sedimentological evidence of an increase in Pseudo-nitzschia (Bacillariophyceae) abundance in response to coastal eutrophication. Limnol. Oceanogr., 47, 551–558, 2002.

Pelletier, J. D.: A spatially distributed model for the long-term suspended sediment discharge and delivery ratio of drainage basins, J. Geophys. Res., 117, F02028, 2012.

Pelletier, G. J., Chapra, S. C., and Tao, H.: QUAL2Kw—A framework for modeling water quality in streams and rivers using a genetic algorithm for calibration. Environ. Model. Softw., 21, 419–425, 2006.

Poesen, J., Boardman, J., Wilcox, B., and Valentin, C.: Water erosion monitoring and experimentation for global change studies, J. Soil Water Conserv., 51, 386–390, 1996.

Popp, A., Calvin, K., Fujimori, S., Havlik, P., Humpenöder, F. et al.: Land-use futures in the shared socio-economic pathways, Global Environ. Change, 42, 331–345, 2017.

Renschler, C. S. and Harbor, J.: Soil erosion assessment tools from point to regional scales—The role of geomorphologists in land management research and implementation, Geomorphology, 47, 189–209, 2002.

Restrepo, J. D., Zapata, P., Díaz, J. M., Garzón-Ferreira, J., and García, C. B.: Fluvial fluxes into the Caribbean Sea and their impact on coastal ecosystems: The Magdalena River, Colombia, Glob. Planet. Change, 50, 33-49, 2006.

Riegman, R.: Nutrient-related selection mechanisms in marine phytoplankton communities and tile impact of eutrophication on the planktonic food web, Water Sci. Technol., 32, 63-75, 1995.

Riley, G. A.: Oceanography of Long Island sound 1952-1954, II. Physical Oceanography, Bull. Bingham. Oceanog. Collection., 15, 15-16, 1956.

Romdhane, M. S., Eilertsen, H. C., Yahia, O. K. D., and Yahia, M. N. D.: Toxic dinoflagellate blooms in Turisian lagoons: causes and consequences for aquaculture, in: Harmful Algae, edited by: Reguera, B., Blanco, J., Fernandez, M. L., and Wyatt, T., Xunta de Galicia and Intergovernmental Oceanographic Commission of UNESCO, Vigo, 80–83, 1998.

Seitzinger, S. P., Mayorga, E., Bouwman, A. F., Kroeze, C., Beusen, A. H. W., Billen, G., Van Drecht, G., Dumont, E., Fekete, B. M., Garnier, J., Harrison, J. A.: Global river nutrient export: A scenario analysis of past and future trends, Global Biogeochem. Cycles, 24, GB0A08, 2010.

Sheffield, J., Goteti, G., and Wood, E. F.: Development of a 50-year high resolution global dataset of meteorological forcings for land surface modeling, J. Clim., 19, 3088–111, 2006.

Shevliakova, E., Pacala, S. W., Malyshev, S., Hurtt, G. C., Milly, P. C. D., Caspersen, J. P., Sentman, L. T., Fisk, J. P., Wirth, C., and Crevoisier, C.: Carbon cycling under 300 years of land use changes: Importance of the secondary vegetation sink, Glob. Biogeochem. Cy., 23, GB2022, 2009.

Sipler, R. E. and Bronk, D. A.: Biogeochemistry of Marine Dissolved Organic Matter, in: Biogeochemistry of Marine Dissolved Organic Matter, edited by: Hansell, D. A. and Carlson, C. A., Academic Press, Kidlington, Oxford, UK, 128-233, 2014.

https://doi.org/10.5194/gmd-2022-236
Preprint. Discussion started: 2 January 2023

Smith, V. H.: Eutrophication of freshwater and coastal marine ecosystems a global problem, Environ. Sci. Pollut. Res., 10, 126–139, 2003.

Smith, S. V., Swaney, D. P., Talaue-Mcmanus, L., Bartley, J. D., Sandhei, P. T., McLaughlin, C. J., Dupra, V. C., Crossland, C. J., Buddemeier, R. W., Maxwell, B. A., and Wulff, F.: Humans, Hydrology, and the Distribution of Inorganic Nutrient Loading to the Ocean, BioScience, 53, 234-245, 2003.

Steele, J. H. and Henderson, E. W., The significance of interannual variability, in: Towards a Model of Ocean Biogeochemical Processes, edited by: Evans, G. T. and Fasham, M. J. R., Springer-Verlag, Berlin, Heidelberg, Germany, 227–260, 1992.

Syvitski, J. P. M., Vörösmarty, C. J., Kettner, A. J., and Green, P.: Impact of humans on the flux of terrestrial sediment to the global coastal ocean, Science, 308, 376–380, 2005.

Tan, Z., Leung, L. R., Li, H., Tesfa, T., Vanmaercke, M., Poesen, J., Zhang, X., Lu, H., and Hartmann, J.: A Global data analysis for representing sediment and particulate organic carbon yield in Earth System Models, Water Resour. Res., 53, 10674–10700, 2017.

Trainer, V. L., Cochlan, W. P., Erickson, A., Bill, B. D., Cox, F. H., Borchert, J. A., Lefebvre, K. A.: Recent domoic acid closures of shellfish harvest areas in Washington State inland waterways, Harmful Algae, 6, 449–459, 2007.

Turner, R. E., Rabalais, N. N., and Justic, D.: Gulf of Mexico hypoxia: alternate states and a legacy, Environ. Sci. Technol., 42, 2323–7, 2008.

Van Beusekom, J. E. E. Eutrophication, in: Handbook on Marine Environment Protection, edited by: Salomon, M. and Markus, T., Springer, Cham, Switzerland, 429-445, 2018.

Van Meter, K. J. and Van Cappellen, P., and Basu, N. B.: Legacy nitrogen may prevent achievement of water quality goals in the Gulf of Mexico, Science, 360, 427–30, 2018.

Vilmin, L., Mogollón, J. M., Beusen, A. H. W., and Bouwman, A. F.: Forms and subannual variability of nitrogen and phosphorus loading to global river networks over the 20th century, Glob. Planet. Change, 163, 67–85, 2018.

Vorosmarty, C. J., Meybeck, M., Fekete, B., Sharma, K., Green, P., and Syvitski, J. P. M.: Anthropogenic sediment retention: major global impact from registered river impoundments, Glob. Planet. Change, 39, 169–190, 2003.

Weind, I., Lotze-Campen, H., Popp, A., Müller, C., Havlík, P., Herrero, M., Schmitz, C., and Rolinski, S.: Livestock in a changing climate: production system transitions as an adaptation strategy for agriculture, Environ. Res. Lett., 10, 094021, 2015.

Zhu, Z., Bi, J., Pan, Y., Ganguly, S., Anav, A., Xu, L., Samanta, A., Piao, S., Nemani, R. R., and Myneni, R. B.: Global Data Sets of Vegetation Leaf Area Index (LAI)3g and Fraction of Photosynthetically Active Radiation (FPAR)3g Derived from Global Inventory Modeling and Mapping Studies (GIMMS) Normalized Difference Vegetation Index (NDVI3g) for the Period 1981 to 2011, Remote Sens., 5, 927-948, 2013.